DEFINING A NOVEL ROLE FOR HYPOXIA INDUCIBLE FACTOR-2 ALPHA (HIF-2α)/EPAS1: MAINTENANCE OF MITOCHONDRIAL AND REDOX HOMEOSTASIS

APPROVED BY SUPERVISORY COMMITTEE:

Joseph A. Garcia, M.D., Ph.D.

Joyce Repa, Ph.D.

Victoria Esser, Ph.D.

Daniel Garry, M.D., Ph.D.

Steven Kliewer, Ph.D.

DEDICATION

To my parents, Gulsum and Cevdet Oktay for their never-ending and invaluable support.

DEFINING A NOVEL ROLE FOR HYPOXIA INDUCIBLE FACTOR-2 ALPHA (HIF-2α)/EPAS1: MAINTENANCE OF MITOCHONDRIAL AND REDOX HOMEOSTASIS

by

YAVUZ OKTAY

DISSERTATION

Presented to the Faculty of the Graduate School of Biomedical Sciences

The University of Texas Southwestern Medical Center at Dallas

In Partial Fulfillment of the Requirements

For the Degree of

DOCTOR OF PHILOSOPHY

The University of Texas Southwestern Medical Center at Dallas

Dallas, Texas

December 2005

ACKNOWLEDGEMENTS

The studies that are described here were made possible by tremendous support and motivation of my mentor Joseph A. Garcia. Also, I would like to thank him for guiding me throughout my studies and helping me improve my scientific skills.

My committee chairman, Joyce Repa, has been greatly helpful with her suggestions and support, I am grateful to her. Victoria Esser is one of the most pleasant scientists I have known and I would like to thank her for her encouragement and friendly approach. I am also thankful to Steven Kliewer for his helpful suggestions with my projects, and for his invaluable support. I would like to thank my former committee member, Cai Li, for his help during his stay. Daniel Garry and Hesham Sadek have also been of great help with technical and theoretical aspects of my project. Marguerite Gunder, Ron Haller and Ronald W. Estabrook provided fantastic support through collaborations or suggestions. I would like to thank Liang-Jun Yan for providing expertise in the field and collaboration. Kosaku Uyeda was very helpful and I learned a lot from him. Marzia Scortegagna and all other members of the Garcia lab have been great to work with and great friends.

DEFINING A NOVEL ROLE FOR HYPOXIA INDUCIBLE FACTOR-2 ALPHA (HIF-2α)/EPAS1: MAINTENANCE OF MITOCHONDRIAL AND REDOX HOMEOSTASIS

YAVUZ OKTAY, Ph.D.

The University of Texas Southwestern Medical Center at Dallas, 2005

Mentor: JOSEPH GARCIA, M.D., Ph.D.

The *Epas1* gene encodes HIF-2α, a member of the Hypoxia Inducible Factor family of transcriptional regulators. The biological role for HIF-2α has been elusive due to embryonic lethality of the initial *Epas1*$^{-/-}$ mouse strains. Our lab reported the generation of the first viable *Epas1*$^{-/-}$ mice using a genetic breeding strategy. Adult *Epas1*$^{-/-}$ mice exhibit gross, histological, biochemical, and

molecular evidence consistent with mitochondrial dysfunction. Similarities between *Epas1* and *Sod2* deficient strains suggest a biochemical etiology, increased oxidative stress, as well as a molecular etiology, decreased *Sod2* gene expression, for the mitochondrial dysfunction in *Epas1*$^{-/-}$ mice. Consistent with this hypothesis, *Sod2* gene expression is reduced in *Epas1*$^{-/-}$ mice whereas HIF-2α induces *Sod2* gene promoter in transient transfection studies. Further studies revealed impaired mitochondrial respiration, sensitized mitochondrial permeability transition pore opening, increased electron transport chain activity and reduced mitochondrial aconitase activity. Given that it is the most sensitive enzymatic marker for oxidative stress, aconitase inhibition may explain impaired respiration. Also, redox balance in *Epas1*$^{-/-}$ liver is disturbed: the reduced cytoplasmic environment, and a relative oxidized environment for mitochondria *from Epas1*$^{-/-}$ liver implies a role for HIF-2α in maintenance of cellular redox balance. All these data suggest that HIF-2α is essential for maintenance of mitochondrial function, reactive oxygen species detoxification, and redox balance.

TABLE OF CONTENTS

Vitae

PRIOR PUBLICATIONS

Oktay Y, Yan LJ, Haller RM, Garcia JA. Cellular and mitochondrial biophysical properties are altered in HIF-2alpha deficient liver. *In preparation.*

Scortegagna M, Ding K, Zhang Q, **Oktay Y**, Bennett MJ, Bennett M, Shelton JM, Richardson JA, Moe O, Garcia JA. Hif-2(alpha) regulates murine hematopoietic development in an erythropoietin-dependent manner. *Blood*, 105(8): 3133-40 (2005).

Scortegagna M, Ding K, **Oktay Y**, Gaur A, Thurmond F, Yan LJ, Marck BT, Matsumoto AM, Shelton JM, Richardson JA, Bennett MJ, Garcia JA. Multiple organ pathology, metabolic abnormalities and impaired homeostasis of reactive oxygen species in Epas1 -/- mice. *Nature Genetics*, 35(4): 331-40 (2003).

Scortegagna M, Morris MA, **Oktay Y**, Bennett M, Garcia JA. The HIF family member EPAS1/Hif-2alpha is required for normal hematopoiesis in mice. *Blood*, 102(5): 1634-40 (2003).

LIST OF FIGURES

LIST OF TABLES

LIST OF ABBREVIATIONS

AhR	Aryl Hydrocarbon Receptor
ARNT	Aryl Hydrocarbon Receptor Nuclear Translocator
Asn	Asparagine
AT(D)P	Adenosine tri(di)phosphate
Bax	BCL2-associated X protein
Bcl2	B-cell leukemia/lymphoma 2
bHLH	Basic helix-loop-helix
Bnip3	BCL2/adenovirus E1B 19kDa interacting protein 3
Cas1	Catalase 1
Cited 2	Cbp/p300-interacting transactivator, with Glu/Asp-rich
COOH-	Carboxyl
COX	Cytochrome oxidase
CTAD	C-terminal activation domain
DEC2	Differentially expressed in chondrocytes 2
DOPS	D,L-threo-3,4-dihydroxyphenylserine
E10	Embryonic day 10
EPAS1	Endothelial PAS Domain Protein 1
Epo	Erythropoietin
Ets1	v-ets erythroblastosis virus E26 oncogene homolog 1
FIH	Factor inhibiting HIF

Gpx1	Glutathione peroxidase 1
GSH	Reduced glutathione
GSSG	Oxidized glutathione
H&E	Hematoxylin and eosin
H_2O_2	hydrogen peroxide
HIF	Hypoxia inducible factor
HRE	Hypoxia response element
lacZ	Gene coding for β-galactosidase
L-DOPA	L-3,4-dihydroxyphenylalanine
MAPK	Mitogen-activated protein kinase
MnSOD	Manganese superoxide dismutase, mitochondrial
MnTBAP	Manganese III tetrakis (5,10,15,20 benzoic acid)
mtPTP	Mitochondrial permeability transition pore
NADH	Nicotinamide adenine dinucleotide hydrogen (reduced)
NH2-	Amino
NLS	Nuclear localization signal
NO	Nitric oxide
NTAD	N-terminal activation domain
NUR	NADH-ubiquinone reductase
ODD	Oxygen-dependent degradation domain
ORO	Oil red O
OZ	Organ of Zuckerkrandl

PAS	Per-ARNT-SIM
PFKFB3	6-phosphofructo-2-kinase/fructose-2,6-biphosphatase 3
PHD	Prolyl Hydroxylase Domain protein
PI3K	phosphatidylinositol 3-kinase
pVHL	von Hippel-Lindau protein
RCR	Respiratory control ratio
ROS	Reactive oxygen species
SDH	Succinate dehydrogenase
SIM	Single-minded
SO	Superoxide
Sod2	Superoxide dismutase 2, the gene coding for MnSOD
UCCR	Ubiquinol:cytochrome c reductase
VEGFR1	Vascular endothelial growth factor receptor 1
ΔΨ	Membrane potential

CHAPTER ONE

GENERAL INTRODUCTION AND LITERATURE REVIEW

PAS domain proteins were first identified in Period (PER) and Single-Minded (SIM) proteins of D. *melanogaster* and Aryl Hydrocarbon Receptor Nuclear Translocator (ARNT) of vertebrates (For a detailed review on PAS domain proteins, see (Taylor and Zhulin 1999) (Figure 1-1a). Members of the PAS domain protein family sense and respond to diverse environmental stimuli including light, redox state, energy state, xenobiotics and hypoxia amongst others. Hypoxia Inducible Factor-2α (HIF-2α), encoded by the Endothelial PAS Domain Protein 1 (*EPAS1*, also known as *HRF, HLF, MOP2*) gene, is a member of basic helix-loop-helix (bHLH)/PAS domain protein family and shows high sequence similarity with HIF-1α, a transcription factor for which a role in the transcriptional response to hypoxia has been extensively studied during the last decade (Figure 1-1b). Both proteins possess a basic DNA-binding domain, helix-loop-helix region, PAS domains, two activation domains (NTAD and CTAD) and an oxygen dependent degradation domain (ODD) (Wang, Jiang et al. 1995; Pugh, O'Rourke et al. 1997; O'Rourke, Tian et al. 1999; Jaakkola, Mole et al. 2001). The similarity between the two proteins is higher at the bHLH and PAS domains, which are responsible for hetero-dimerization with ARNT, and lower at NTAD, CTAD and ODDs. Therefore, it was postulated that HIF-1α and HIF-2α may bind different transcriptional co-activators and may be differentially regulated by various stimuli, including oxygen, nitric oxide (NO), redox state, and reactive

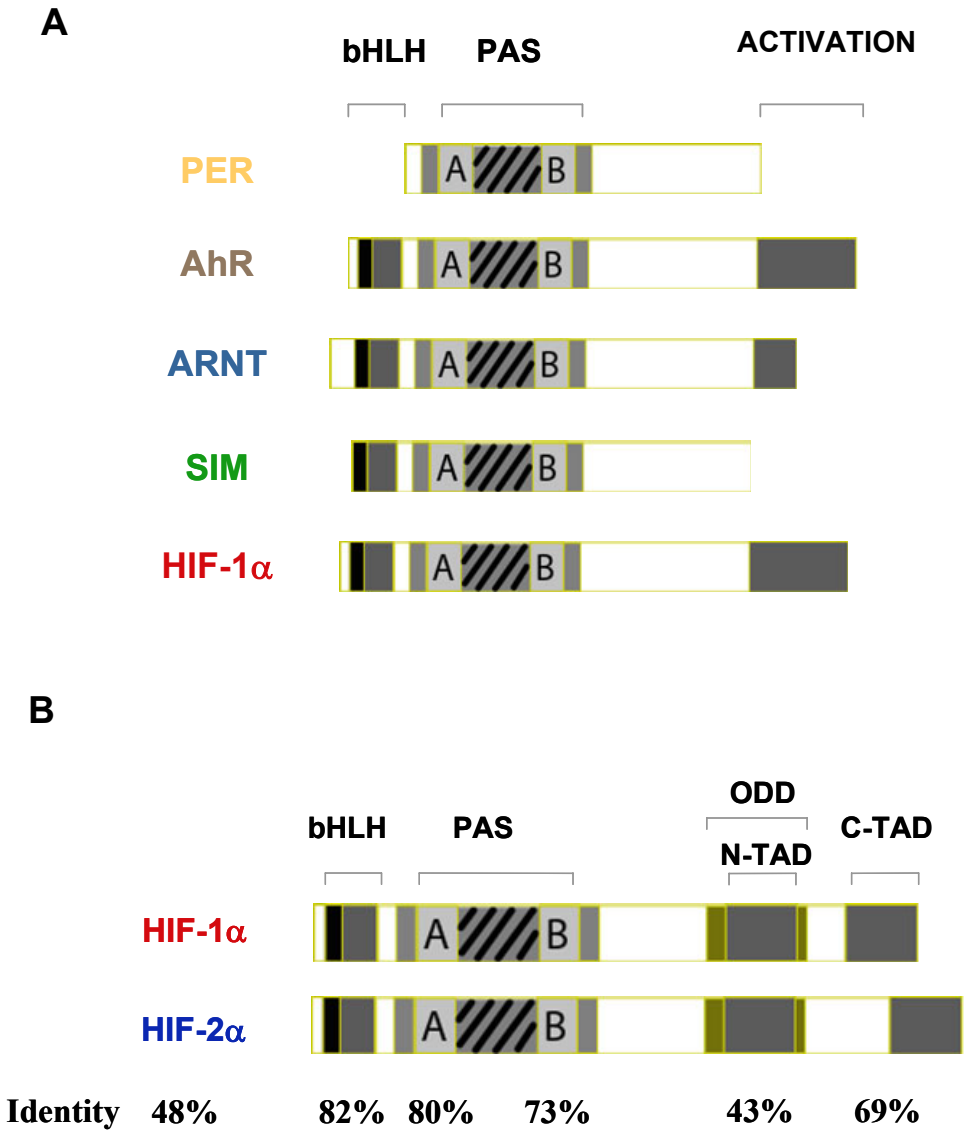

Figure 1-1. PAS domain proteins and comparison of HIF-1α and HIF-2α members.
A. Founding members of the PAS domain family of proteins: Period (PER), AhR (Aryl Hydrocarbon Receptor), ARNT (Aryl Hydrocarbon Receptor Nuclear Translocator) and SIM (Single-Minded) of D. *melanogaster*. Each domain has two PAS repeats, "A" and "B". ***B.*** Comparison of human HIF-1α and HIF-2α. The identity between two proteins is higher in DNA-binding and dimerizing NH_2- terminal domains; lower similarity at COOH- terminal domains may indicate differential regulation and target specificity. Identity between the two amino-acid sequences was determined with the BLAST program at http://www.ncbi.nih.gov/BLAST/.

oxygen species (ROS) (Wang, Jiang et al. 1995; Richard, Berra et al. 2000; Hu, Wang et al. 2003; Bardos and Ashcroft 2005; Wang, Davis et al. 2005). However, until recently, a majority of the studies in the HIF field has focused on the role of HIF-1α in hypoxic stress response and its regulation by oxygen.

Regulation of HIF-1α and HIF-2α

HIF-1α was identified by its binding to the Erythropoietin (Epo) enhancer under low oxygen conditions (Semenza and Wang 1992). Following studies established HIF-1α as a master regulator of transcriptional responses to low oxygen levels (Wang, Jiang et al. 1995; Iyer, Kotch et al. 1998; Jaakkola, Mole et al. 2001). HIF-2α and HIF-3α are also oxygen sensitive subunits of HIF-2 and HIF-3, respectively. HIF-1β (also known as ARNT) subunit is shared by HIF-1α, HIF-2α and HIF-3α. HIF-β is constitutively expressed and is not subject to oxygen dependent degradation due to the absence of an ODD. HIF-2α regulation by oxygen is similar to HIF-1α, as described below (Figure 1-2).

HIF-1α and HIF-2α are recognized by Prolyl Hydroxylase Domain (PHD) proteins, PHD1-3, under normoxic conditions and specific proline residues (Proline 402 and 564 of human HIF-1α, and proline 405 and 531 of human HIF-2α) in the ODD are hydroxylated by PHDs. PHD activity is dependent on oxygen, Fe(II) and 2-oxoglutarate, a Krebs Cycle intermediate (Bruick and McKnight 2001; Epstein, Gleadle et al. 2001). Hydroxylated prolines are

recognized by the tumor suppressor protein von Hippel-Lindau (pVHL), an E3 ligase component (Maxwell, Wiesener et al. 1999) and subsequently HIFα subunit is degraded by the proteasome. Under hypoxic conditions, PHDs are inhibited, thereby allowing HIFα members to escape degradation and become transcriptionally active.

Although oxygen-dependent regulation of HIFs is well understood now, due to the recent progress involving identification and characterization of PHDs, regulation of HIFs by other stimuli such as mitochondrial/cytosolic reactive oxygen species (ROS) and redox state is less clear (Salceda and Caro 1997; Chandel, Maltepe et al. 1998; Ema, Hirota et al. 1999; Agani, Pichiule et al. 2000; Chandel, McClintock et al. 2000; Lando, Pongratz et al. 2000; Schroedl, McClintock et al. 2002; Gong and Agani 2005).

Physiological Roles of HIFs

HIF-1α mediates the transcriptional response to hypoxic stress by induction of several genes involved in **glycolysis** (*Glucokinase*, *Aldolase A, Phosphoglycerate Kinase 1, Lactate Dehydrogenase A, PFKFB3, Enolase 1)*, **glucose uptake** (Glucose Transporter 1), **angiogenesis** (*Vascular Endothelial Growth Factor, Flt-1/VEGFR1*), **oxygen supply** (*Globin 2, Plasminogen Activator Inhibitor 1, Inducible and Endothelial Nitric Oxide Synthases*), **iron metabolism** (*Transferrin, Transferrin Receptor, Ceruloplasmin*), **cell proliferation/apoptosis** (*Insulin like Growth Factor Binding Protein 1, BNip3*) and **others** (*DEC2, Cited2,*

Ets1) (Wenger, Stiehl et al. 2005). The number and variety of HIF-1α target genes implies a major role for HIF-1α in mediating a hypoxia response pathway at systemic, local and intracellular levels (Semenza 2004). However, these studies were performed mostly in cell-culture models and, therefore, their physiological relevance was limited.

In comparison to HIF-1α, HIF-2α is able to induce only a subset of those genes regulated by HIF-1α. For example, both HIF-1α and HIF-2α are able to induce VEGF and Glut1 in response to hypoxia, but only HIF-1α can induce expression of glycolytic genes (Hu, Wang et al. 2003). Therefore, despite sharing high sequence identity, their regulation and target gene profiles are not completely overlapping. Temporal and spatial expression of HIF-1α and HIF-2α are also quite different: HIF-1α is ubiquitously expressed, whereas HIF-2α expression in rats is restricted to fetal lung, heart, and liver parenchyma, as well as the adult liver, intestine, cardiac myocytes, kidney epithelial cells, bone marrow, uterine decidual cells and pancreas (Wiesener, Turley et al. 1998; Ema, Hirota et al. 1999; Wiesener, Jurgensen et al. 2003).

Gene targeting in animal models such as mouse is an extensively used strategy to understand developmental and physiological roles of targeted genes. However, embryonic lethality of *HIF-1α*$^{-/-}$ and *Epas1*$^{-/-}$ mice hampered studies on the physiologic roles of HIF-1α and HIF-2α (Tian, McKnight et al. 1997; Iyer, Kotch et al. 1998; Ryan, Lo et al. 1998; Peng, Zhang et al. 2000; Compernolle, Brusselmans et al. 2002). *HIF-1α*$^{-/-}$ embryos show morphological abnormalities

starting at E8.5 and die by E11; they show cardiovascular and neural tube defects with marked cell death in the cephalic mesenchyme. On the other hand, *Epas1*$^{-/-}$ embryos die between E12.5 and E16.5 with no morphological abnormalities. *Epas1*$^{-/-}$ embryos showed normal vascular development, but pronounced bradycardia near death, with low levels of catecholamines contributing to embryonic lethality.

Although, differences in spatial and temporal regulation of HIF-1α and HIF-2α expression may in part explain the differing embryonic lethal phenotypes of *Epas1*$^{-/-}$ and *HIF-1*$\alpha^{-/-}$ mice, several lines of evidence point to distinct roles for HIF-1α and HIF-2α including differences in stimuli specificity, target gene selectivity, sub-cellular localization, and protein stability. It is now recognized that HIF-2α is not merely a paralog of HIF-1α. Recently, a breeding strategy used by our group, mating of isogenic 129S6/SvEvTac and congenic C57BL/6J mice heterozygous for the Epas1 gene, yielded viable *Epas1*$^{-/-}$ progeny (Scortegagna, Ding et al. 2003). We were interested in understanding the unique physiological roles of HIF-2α in surviving *Epas1*$^{-/-}$ juvenile mice. Studies on these viable *Epas1*$^{-/-}$ mice will be the focus of Chapters 2 and 3.

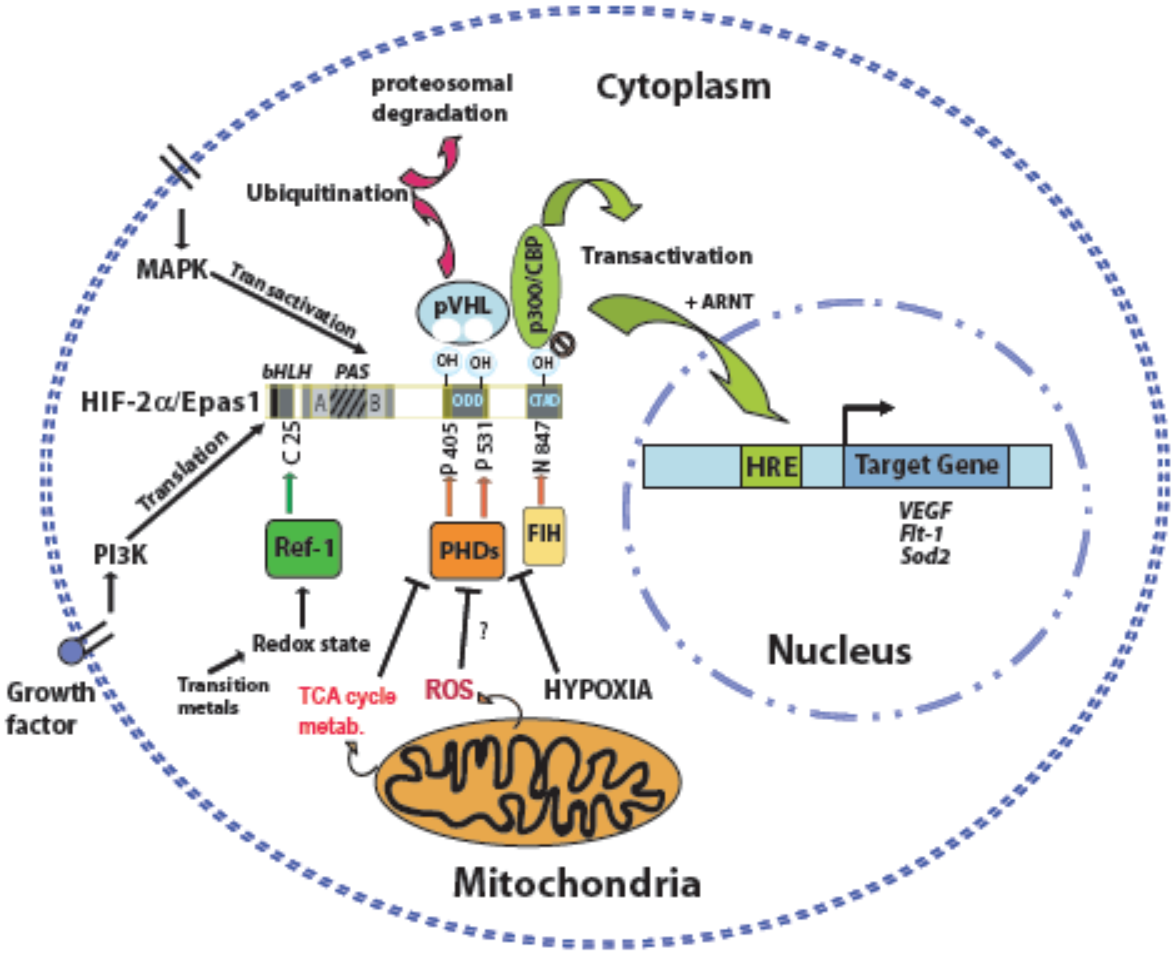

Figure 1-2. Regulation of HIF-2α activity by oxygen, ROS and other stimuli.
Under normal oxygen pressure, HIF-1α and HIF-2α are hydroxylated by Prolyl Hydroxylase Domain (PHD) proteins at two proline residues (Pro405 and Pro531 of human HIF-2α). Hydroxylated prolines are recognized by von Hippel-Lindau (VHL), a component of an E3 ubiquitin ligase complex, and subsequently targeted for proteosomal degradation. Hypoxia and other stimuli inhibit PHDs and lead to stabilization of HIF-1α and HIF-2α. Stabilized HIF-2α translocates to nucleus with its dimerization partner, ARNT, and binds to hypoxia response elements (HREs) within their target genes. Factor Inhibiting HIF (FIH) hyroxylates a specific asparagines residue (Asn 847 of HIF-2α) in CTAD and inhibits its interaction with p300/CBP transcriptional co-activator, which is required for full-activity of HIFs. Redox state modulates HIF-2α but not HIF-1α DNA-binding via a cysteine residue (Cys 25) in the bHLH domain of HIF-2α.

CHAPTER TWO

Epas1$^{-/-}$ MICE EXHIBIT STRAIN DEPENDENT SURVIVAL, MULTIPLE ORGAN PATHOLOGY AND METABOLIC ABNORMALITIES

Introduction:

To understand developmental and physiological roles of HIF-1α and HIF-2α in animals, knock-out mice strategies were employed by several research groups. However, embryonic lethality of both *HIF-1*$\alpha^{-/-}$ and *Epas1*$^{-/-}$ mice hampered studies on the physiological roles of HIF-1α and HIF-2α (Tian, McKnight et al. 1997; Iyer, Kotch et al. 1998; Ryan, Lo et al. 1998; Peng, Zhang et al. 2000; Compernolle, Brusselmans et al. 2002).

High-level expression of HIF-1α in mouse embryo starts between E8.5 and E9.5 during embryogenesis. *HIF-1*$\alpha^{-/-}$ embryos reveal developmental arrest, morphological abnormalities as early as E8.5 and eventually die between E10 - E11. Complete deficiency of HIF-1α causes cardiovascular malformations, neural tube defects and cell death within the cephalic mesenchyme (Iyer, Kotch et al. 1998). The presence of enlarged vascular structures are similar to those observed in vascular endothelial growth factor (*VEGF*$^{-/-}$) embryos (Carmeliet, Ferreira et al. 1996), suggesting that HIF-1α is required for VEGF expression and vascular development at least during certain stages of development. Although analysis of *HIF-1*$\alpha^{-/-}$ embryos provided important information about the

developmental roles of HIF-1α, our knowledge of physiological roles for HIF-1α in adult physiology remained limited.

On the other hand, *HIF-1α*$^{+/-}$ mice develop normally and do not show any overt phenotype. However, exposure to long-term hypoxia (10%, 3 weeks) causes increased right ventricular hypertrophy, pulmonary hypertension and delayed development of erythrocytes in these mice (Yu, Shimoda et al. 1999). These studies confirm the importance of HIF-1α for systemic responses to hypoxia.

The embryonic lethality of HIF-1α knockout mice was circumvented by the recent development of a conditional knockout strain. Tissue-restricted elimination of HIF-1α has allowed investigators to define the role of HIF-1α in specific biological processes. For example, monocytes lacking HIF-1α are unable to induce the glycolytic burst normally observed upon antigen activation (Cramer, Yamanishi et al. 2003). These studies confirm HIF-1α as a master regulator of glycolytic gene expression and hence of glycolysis, results also observed with *HIF-1α*$^{-/-}$ mouse embryonic fibroblast studies (Seagroves, Ryan et al. 2001). Additional studies using tissue-restricted elimination of HIF-1α provided substantial information on physiological roles of HIF-1α (Maxwell 2005) (See Table 2-1). HIF-1α is required for cardiovascular development, chondrogenesis, adipogenesis, B lymphocyte and mammary gland development, angiogenesis, glycolysis, hypoxia-induced erythropoiesis, cell cycle arrest and apoptosis, pulmonary vascular remodeling, carotid body sensing of arterial oxygen

pressure, inflammation, and myocardial preconditioning (Semenza 2004; Maxwell 2005).

Table 2-1. Tissue-restricted inactivation of HIF-1α in mice and corresponding phenotypes. *Adapted from (Maxwell 2005).*

Control sequence used to drive Cre recombinase expression	Cell population	Phenotype	Reference
Lymphocyte specific protein-tyrosine kinase; Lck	T cells	Resistance to apoptosis in thymus	(Biju *et al.* 2004)
Lysozyme M	Myeloid lineage	Decreased inflammatory and antimicrobial responses	(Cramer *et al.* 2003) (Cramer *et al.* 2003)
Muscle creatine kinase	Skeletal muscle	Increased endurance, prone to muscle damage	(Mason *et al.* 2004)
Fatty acid binding protein	Colonic epithelium	Decreased intestinal barrier function	(Karhausen *et al.* 2004)
Myosin light chain 2, MLC2v	Cardiac myocyte	Contractile dysfunction	(Huang *et al.* 2004)
Calcium/calmodulin-dependent kinase CaMKIIα	Neurones	Protection from hypoxia-induced cell death	(Helton *et al.* 2005)
Collagen2A1 (α1 chain of type II collagen)	Chondrocytes	Defective growth arrest in bone growth plates	(Schipani *et al.* 2001)
Mouse mammary tumour virus (MMTV)	Mammary epithelium	Impaired mammary differentiation and lipid secretion	(Seagroves *et al.* 2003)

On the other hand, over-expression of constitutively active human HIF-1α that lacks the ODD (HIF-1α(401Δ603)) in mouse epidermal keratinocytes resulted in hypervascularity, leakage resistance, and upregulation of VEGF mRNA and protein (Elson, Thurston et al. 2001). The authors concluded that epithelial hypoxia, particularly HIF-1α activity, may mediate induction of leakage resistant vasculature. In contrast to HIF-1α, limited knowledge regarding the biological role of HIF-2α has been obtained from embryonic and tumor cell line studies (Hu, Wang et al. 2003; Park, Dadak et al. 2003).

Epas1$^{-/-}$ mice generated by three different groups showed embryonic lethality (Tian, McKnight et al. 1997; Peng, Zhang et al. 2000; Compernolle, Brusselmans et al. 2002). However, the proposed causes of embryonic death were varied: catecholamine deficiency and bradycardia (Tian, McKnight et al.

1997), disruption of vascular remodeling (Peng, Zhang et al. 2000), and respiratory distress syndrome due to impaired surfactant protein production in lungs (Compernolle, Brusselmans et al. 2002). It is not clear why different mouse lines exhibit different phenotypes; however, it is likely to be due to different targeting strategies and/or background genetic effects.

The *Epas1*$^{-/-}$ mice that are described below were obtained from the original 129S6/SvEvTac isogenic strain deficient for one allele of HIF-2α, generated by the McKnight lab, crossed to a congenic C57BL/6J strain generated by the Garcia lab, to yield F1 hybrid mice replete or deficient in *Epas1*. The original targeting strategy of *Epas1* is outlined in Figure 2-1. *Epas1*$^{+/-}$ mice did not have gross morphological phenotype and were indistinguishable from their *Epas1*$^{+/+}$ littermates. However, *Epas1*$^{-/-}$ embryos started dying as early as E12.5 and none survived beyond E16.5.

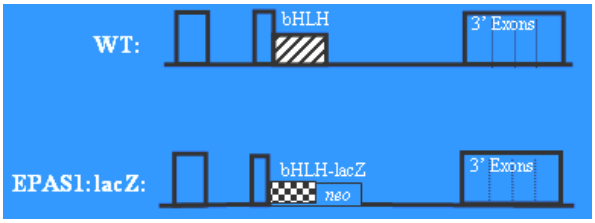

Figure 2-1. Mutation of *EPAS1* gene. E. *coli lacZ* gene replacing exon2 of *EPAS1*. First 13 nucleotides of bHLH exon was fused in-frame to *lacZ* gene with a nuclear localization signal (NLS).

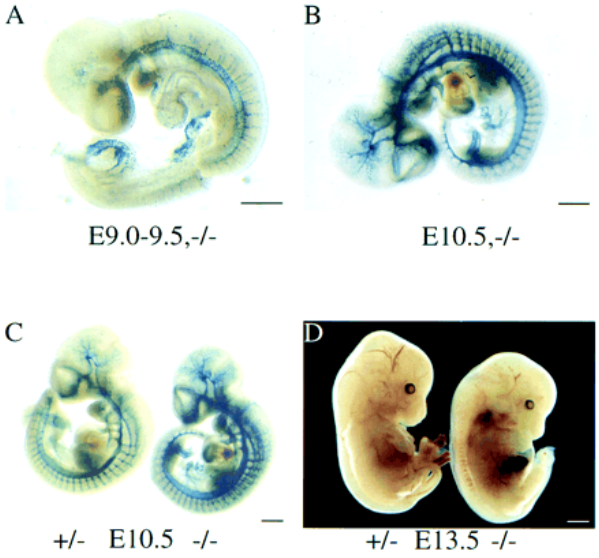

Figure 2-2. Expression of lacZ surrogate marker in vasculature. LacZ staining was followed during angiogenesis stages of embryo (A-C). Beginning at E9.0 lacZ expression can be observed in the dorsal aorta and intersegmental arteries. Vascular development is not affected in *Epas1*$^{-/-}$ embryos. (D) Congested blood is apparent in fetal liver at E13.5.
From (Tian, Hammer et al. 1998)

Interestingly, between E12.5 and E16.5, no morphological abnormality was observed in *Epas1*$^{-/-}$ embryos that survived. Vascular development was not affected by deficiency of HIF-2α, suggesting that HIF-2α is not required during embryonic vasculogenesis. Analysis of liver, heart and skeletal muscle between E11.5 - E15.5 did not show any morphological defect, either. These findings hint at a physiological defect, rather than a developmental defect, in *Epas1*$^{-/-}$ embryos. *Epas1*$^{-/-}$ mice on the 129S6/SvEvTac background also yielded similar results.

High expression levels of HIF-2α in the Organ of Zuckerkrandl (OZ) (Figure 2-3), the primary site of embryonic catecholamine production, suggested that catecholamine deficiency as a possible cause of death for *Epas1*$^{-/-}$ embryos. Supporting this hypothesis, authors observed lower norepinephrine levels and bradycardia in *Epas1*$^{-/-}$ embryos (Tian, Hammer et al. 1998).

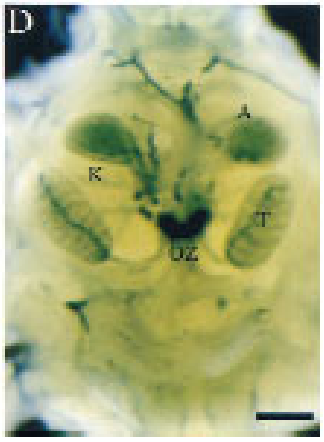

Figure 2-3. High-level expression of HIF-2α in the Organ of Zuckerkrandl (OZ) at E15.5.
OZ is the main site of catecholamine production during embryonic development.
K: Kidney, A: Adrenal, T: Testis, Bar: 50 μm
Adapted from (Tian, Hammer et al. 1998)

To test their hypothesis, Tian and colleagues treated pregnant females with L-DOPA or DOPS, which are norepinephrine precursors by different pathways, and they observed rescue of embryonic lethality by 40% with DOPS but none with L-DOPA (Tian, Hammer et al. 1998). However, viable rescued pups failed to suckle and died within a day after birth. Although these studies indicated an essential role for HIF-2α during embryonic development and fetal physiology, our knowledge of HIF-2α in juvenile/ adult animal physiology remained limited.

In subsequent efforts, the Garcia lab obtained viable *Epas1*$^{-/-}$ mice by breeding a congenic C57BL/6J strain heterozygous for the *Epas1:lacZ* allele with an 129S6/SvEvTac strain heterozygous for the *Epas1:lacZ* allele. Viable F_1 progeny (~5 % of total viable progeny) were analyzed at 4 weeks of age and the data we obtained provided significant and relatively unexpected insights into the roles of HIF-2α in juvenile/adult animal physiology.

Results

Strain dependent survival of Epas1$^{-/-}$ *mice*

Congenic C57BL/6J mice heterozygous for the Epas1:null allele (*C57- Epas1*$^{+/-}$) were generated by repeated backcrossing of mice heterozygous for Epas1-null allele to wild-type C57BL/6J mice. *129- Epas1*$^{+/-}$ mice were generated as described (Tian, McKnight et al. 1997). *129- Epas1*$^{+/-}$ x *129- Epas1*$^{+/-}$ or *C57- Epas1*$^{+/-}$ x *C57- Epas1*$^{+/-}$ crosses did not yield any viable progeny (Figure 2-4 and Table 2-2). Also, *C57- Epas1*$^{+/-}$ x *C57- Epas1*$^{+/-}$ cross yielded mice

heterozygous for Epas1-null allele at less than 2:1 expected Mendelian ratio, indicating a haploinsufficient effect of the C57BL/6J genetic background. There were no surviving *Epas1*$^{-/-}$ mice from isogenic 129S6/SvEvTac or congenic C57BL/6J self-mating. Only F_1 hybrid mating yielded viable *Epas1*$^{-/-}$ mice (~ 5 % of total viable progeny). Due to postnatal mortality, the life span of juvenile *Epas1*$^{-/-}$ mice was substantially lower by two months of age (Figure 2-5).

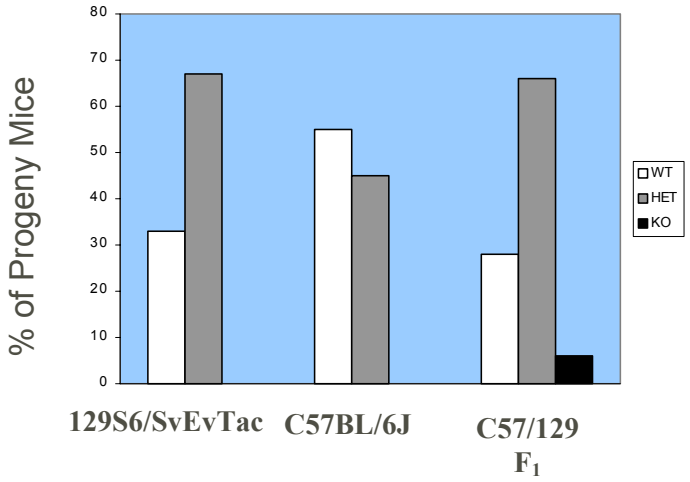

Figure 2-4. Strain dependent survival of *Epas1*$^{-/-}$ mice.
Only F_1 hybrid mating yields viable *Epas1*$^{-/-}$ progeny. White bars indicate wild-type, grey bars indicate *Epas1*$^{+/-}$ and black bar indicates *Epas1*$^{-/-}$ mice. *Adapted from (Scortegagna, Ding et al. 2003)*

Table 2-2. Strain dependent survival *of Epas1*$^{-/-}$ mice.
Only F_1 hybrid mating yields viable *Epas1*$^{-/-}$ progeny

Mating Pair	(+/+)/Total Mice	(+/-)/Total Mice	(–/–)/Total Mice
129 $^{+/-}$ x 129 $^{+/-}$	72/221 (33%)[a]	149/221 (67%)[a]	0/221 (0%)[a]
C57 $^{+/-}$ x C57 $^{+/-}$	44/80 (55%)[a]	36/80 (45%)	0/80 (0%)[a]
C57 $^{+/-}$ x 129 $^{+/-}$	186/670 (28%)[b]	440/670 (66%)[a]	44/670 (6%)[a]
Predicted	(25%)	(50%)	(25%)

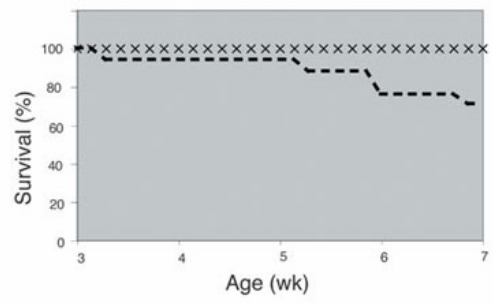

Figure 2-5. Kaplan-Meier survival curve of Epas1$^{-/-}$ mice.
Juvenile Epas1$^{-/-}$ mice show decreased life-span. Wild-type mice are indicated by "X", and *Epas1*$^{-/-}$ mice by "-". *Adapted from (Scortegagna, Ding et al. 2003)*

Epas1$^{-/-}$ mice has smaller stature, fewer spontaneous movements and decreased hang time in a grip-strength test (Figure 2-6 and data not shown). *Epas1*$^{-/-}$ male and female mice were also sterile (data not shown).

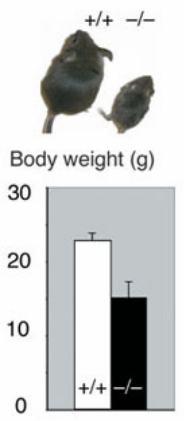

Figure 2-6. Reduced stature of *Epas1*$^{-/-}$ mice. *Epas1*$^{-/-}$ mice are smaller during and after birth. One month old mice are shown. Adapted from (Scortegagna, Ding et al. 2003)

Cardiac hypertrophy, steatotic hepatomegaly and lipid deposits in various tissues

Analysis of *Epas1*$^{-/-}$ mice at one month of age revealed overt cardiac hypertrophy with enlarged cardiac myofibrils, enlarged liver with microvesicular and macrovesicular steatosis and lipid deposits in heart and skeletal muscle (Figure 2-7). Lipid deposits may be indicative of impaired fatty acid oxidation, synthesis or transport. However, further studies support the first explanation (Figure 2-8). The liver was the most severely affected organ with the highest levels of lipid deposits.

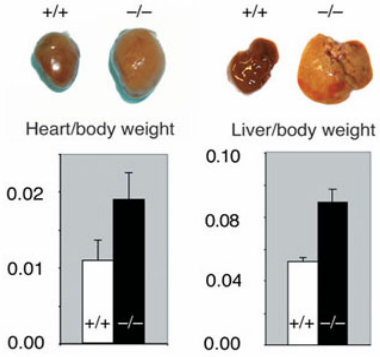

Figure 2-7. Cardiac hypertrophy and hepatomegaly with steatosis in *Epas1*$^{-/-}$ mice. Despite reduced stature, *Epas1*$^{-/-}$ mice show increased heart/body weight and liver/body weight ratios. Lipid accumulation causes paler heart and liver. *Adapted from (Scortegagna, Ding et al. 2003)*

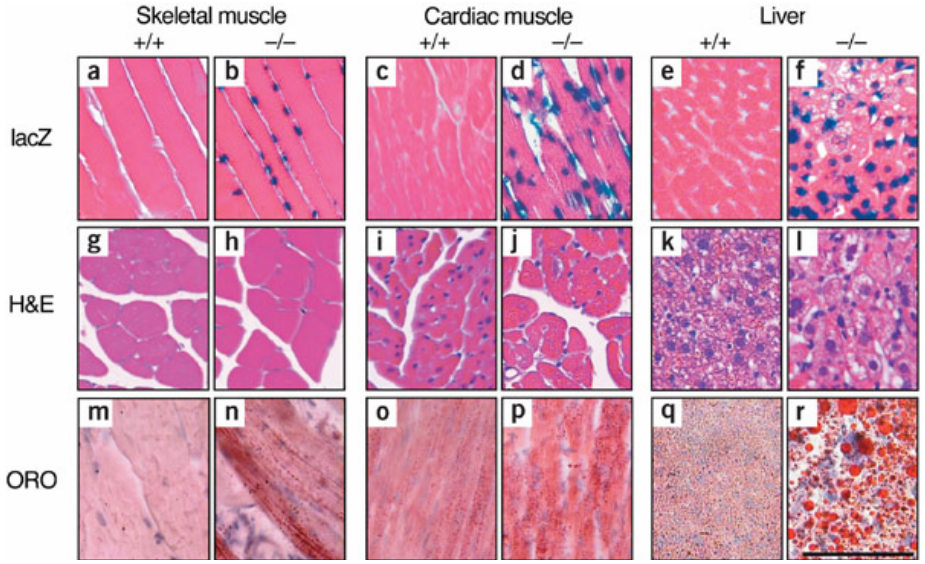

Figure 2-8. *Epas1:lacZ* expression and histological examination.
(a-f) Epas1 is expressed in parenchymal cells of liver, heart and skeletal muscle of one month old mice, (g-l) H&E staining reveals enlarged cardiac myofibrils with inclusions, (m-r) oil red O (ORO) staining reveals increased lipid deposits in liver, heart and skeletal muscle. *Adapted from (Scortegagna, Ding et al. 2003)*

In addition to liver, heart and skeletal muscle, other tissues including eye, bone and testis are affected in *Epas1*$^{-/-}$ mice: retinopathy with reduced photoreceptor layers, pancytopenia (reduced number of white and red blood cells, as well as platelets), and fewer mature spermatids (data not shown) (Scortegagna, Ding et al. 2003). *lacZ* surrogate marker was expressed in all affected organ/tissues. However, no overt pathology was observed in brain despite *lacZ* expression in vascular endothelial and non-neuronal cells of brain.

Altered acyl-carnitine profiles suggests impaired fatty acid oxidation

Impaired fatty acid oxidation may cause lipid accumulation such as that observed in various tissues of *Epas1*$^{-/-}$ mice. Analysis of plasma acyl-carnitine profiles revealed increased C16:C2 ratio and intermediate acyl-fatty acid species

in *Epas1*$^{-/-}$ mice compared to wild-type mice (Scortegagna, Ding et al. 2003). This pattern is strikingly similar to those observed in patients with impaired fatty-acid oxidation.

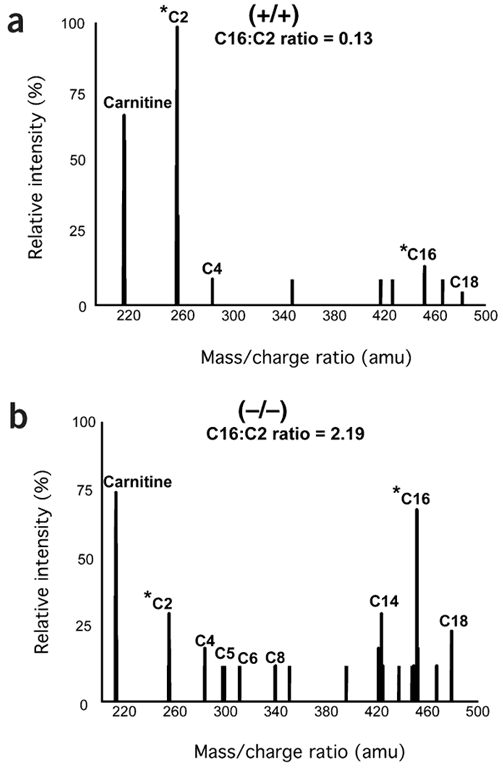

Figure 2-9. Altered serum acyl-carnitine profile of *Epas1*$^{-/-}$ mice. Tandem mass spectroscopy of serum acyl-carnitines indicates increased C16:C2 ratio and intermediate acyl-fatty acids, suggesting impaired fatty acid oxidation in *Epas1*$^{-/-}$ mice. Adapted from (Scortegagna, Ding et al. 2003).

Serum/urine chemistries

Serum and urine chemistry analyses revealed hypoglycemia, anion-gap acidosis and increased serum lactate levels (Table 2-3). Moreover, relative ratios of Krebs cycle intermediates are altered and ketone bodies are present in urine of *Epas1*$^{-/-}$ mice, supporting a mitochondrial disease state. Additionally, serum sodium, potassium, creatinine and catecholamine levels are not affected in *Epas1*$^{-/-}$ mice, suggesting normal adrenal and renal function (data not shown).

Table 2-3. Biochemical abnormalities in *Epas1*$^{-/-}$ mice.
Serum and urine chemistry analysis indicates altered Krebs Cycle, ketogenesis, lactate accumulation and hypoglycemia. a, $p < 0.05$; b, $p < 0.10$
Adapted from (Scortegagna, Ding et al. 2003)

	+/+	-/-
Serum chemistries (mmol/l):		
glucose	12.4 ± 0.6	5.0 ± 0.5[a]
lactate	3.3 ± 0.2	18.3 ± 1.4[a]
Urine chemistries (relative ratios):		
lactate	1.7 ± 0.4	90.5 ± 20.6[a]
citrate / isocitrate	6.1 ± 1.0	4.7 ± 1.0
aconitate	5.0 ± 0.9	3.1 ± 0.4[a]
glutarate	1.1 ± 0.2	1.0 ± 0.3
succinate	10.2 ± 1.5	3.9 ± 0.8[a]
fumarate	1.1 ± 0.3	5.8 ± 1.1[a]
malate	0.4 ± 0.1	1.8 ± 0.5[a]
4-hydroxyphenyl-lactate	0.2 ± 0.1	3.8 ± 0.5[a]
4-hydroxyphenyl-pyruvate	1.2 ± 0.2	8.4 ± 1.3[a]
ketones	0	35.8 ± 9.4[a]

.

Discussion

This study provided the first viable animal model for analysis of HIF-2α function in juvenile animal physiology. Histological and biochemical analysis of *Epas1*$^{-/-}$ mice identified several strain-dependent effects of HIF-2α deficiency. *Epas1*$^{-/-}$ mice had clear differences in survival on the F_1 background versus the 129 or C57 background, similar to the synergistic effect observed in F_1 hybrids of some other knockout mouse models (including the Superoxide Dismutase 2 (*Sod2*)$^{-/-}$ knockout model (Huang, Carlson et al. 2001)). Juvenile *Epas1*$^{-/-}$ mice had multiple organ pathology and a high mortality rate. The immediate cause of death for *Epas1*$^{-/-}$ mice is unknown, but metabolic crisis is a possible etiology.

Essentially normal catecholamine levels in one month old *Epas1*$^{-/-}$ mice suggest that the pathologies observed are not due to catecholamine deficiency. Instead, the widespread pathology and altered metabolic profiles observed in *Epas1*$^{-/-}$ mice suggested a systemic metabolic disorder, possibly due to mitochondrial dysfunction. Therefore, our following studies focused on mitochondrial dysfunction in *Epas1*$^{-/-}$ mice and its possible etiologies.

CHAPTER THREE

IMPAIRED MITOCHONDRIAL AND REDOX HOMEOSTASIS IN *Epas1*$^{-/-}$ MICE

Introduction

As described in the previous chapter, we succeeded in generating the first viable global knockouts of *Epas1* using a genetic breeding strategy (Scortegagna, Ding et al. 2003). *Epas1*$^{-/-}$ mice that survive to adulthood develop hepatomegaly with steatosis, cardiac hypertrophy, skeletal myopathy, lactic acidosis, hypoglycemia and impaired fatty acid oxidation by one-month of age. These aspects of the *Epas1*$^{-/-}$ phenotype are similar to those found in mitochondrial disease conditions. Therefore, we hypothesized that HIF-2α is essential for mitochondrial function and we sought to explore this hypothesis.

To understand mitochondrial pathophysiology, it is crucial to understand oxidative phosphorylation (OXPHOS) (Wallace 2001). Most differentiated cells depend on mitochondria for energy production via OXPHOS. Therefore, any defect in the OXPHOS process may lead to severe impairment of cellular functions.

Electrons generated by fuel oxidation are transferred to NAD^+ to produce NADH. This process occurs through glycolysis in cytosol and Krebs Cycle in mitochondria. Eventually electrons are transferred to the Electron Transport Chain (ETC) at complex I (NADH-ubiquinone oxidoreductase) or at complex II (succinate dehydrogenase) (Figure 3-1). The next carrier is ubiquinone

(Coenzyme Q), which transfers electrons to complex III (ubiquinol-cytochrome c oxidoreductase). Complex III transfers electrons to cytochrome c and cytochrome c passes them to complex IV (cytochrome c oxidase, COX). The final acceptor of electrons is ½ O_2, to yield H_2O. Transfer of electrons through ETC is coupled to the pumping of H^+ ions out into the intermembrane space, thereby creating an electrochemical potential (ΔΨ). ΔΨ drives the synthesis of ATP from ADP by complex V (ATP synthase) or transport of metabolites/ions into/ or out of the mitochondrial matrix.

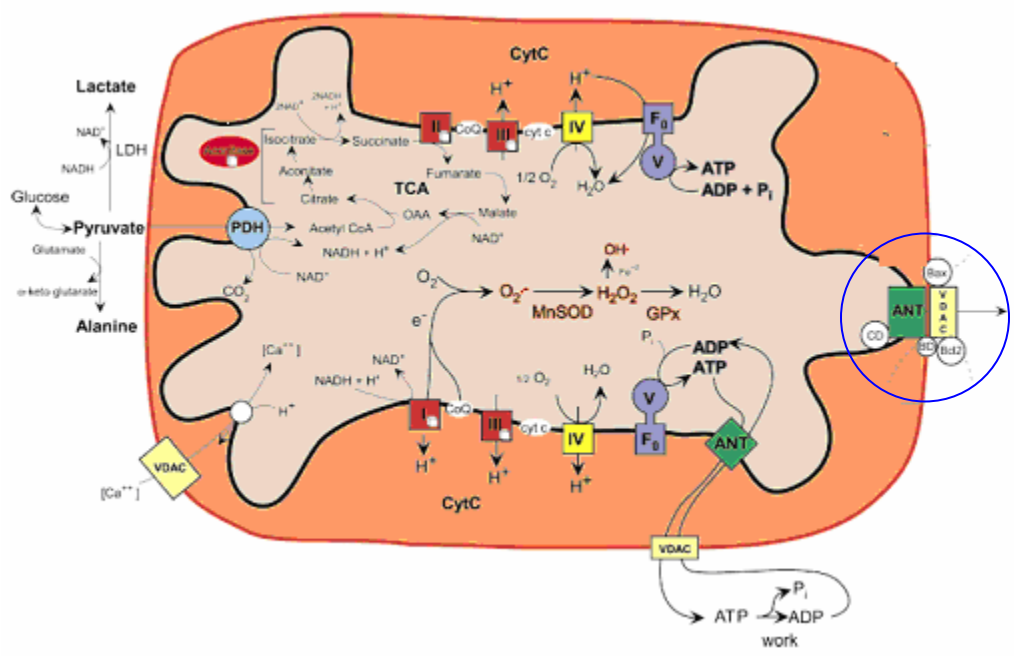

Figure 3-1. Mitochondrial OXPHOS and its relations to AT and ROS production, and mtPTP opening

Acetly-CoA is generated by pyruvate dehydrogenase (PDH) and fatty acid oxidation. NADH generated from acetyl-CoA during Krebs Cycle (also known as TCA Cycle) donates electrons to complex I of ETC. ROS are generated as a byproduct of electron transfer and is converted to H_2O_2 by MnSOD/Sod2 and the resulting H_2O_2 is converted to H_2O by glutathione peroxidase 1(GPx1).

ETC components with Fe-S centers, aconitase and α-KGDH are sensitive to ROS inactivation (red colored). Permeability transition pore (mtPTP, indicated by a blue circle) is also sensitive to ROS and pathophysiological opening of mtPTP may lead to inhibition of OXPHOS and eventually to cell death. ROS sensitive proteins/complexes are in red.

Adapted from (Wallace 2001)

However, electron transfer through ETC does not exhibit 100% efficiency and 0.5-5 % of electrons escape and are transferred to O_2, to form superoxide (SO) anion ($O_2^{\cdot-}$). Fe-S centers of complexes I, II and III, and the Krebs cycle enzyme aconitase are sensitive to reactive oxygen species (ROS) including superoxide. Therefore, impaired ability of mitochondria to remove superoxide under pathophysiological conditions may lead to damage of ETC complexes and/or aconitase. Manganese dependent superoxide dismutase (MnSOD encoded by *Sod2* gene) is responsible for converting SO to H_2O_2, which is then reduced to H_2O by glutathione peroxidase 1 (GPx1) or catalase. Interestingly, *Sod2*$^{-/-}$ mice are phenothypically very similar to *Epas1*$^{-/-}$ mice, including pathological features of prenatal lethality, retinopathy, hepatic steatosis, cardiac hypertrophy, infertility and anemia (Li, Huang et al. 1995; Lebovitz, Zhang et al. 1996; Friedman, Rebel et al. 2001; Huang, Carlson et al. 2001).

Another important function of mitochondria is to regulate apoptosis through opening of the Mitochondrial Permeability Transition Pore (mtPTP). (Figure 3-1) mtPTP is a large complex composed of the inner membrane Adenine Nucleotide Translocase (ANT), outer membrane Voltage-Dependent Anion Channel (VDAC), Bax, Bcl-2, cyclophilin D, and benzadiazopine receptor (Zoratti and Szabo 1995; Wallace 2001). Physiological opening of mtPTP eliminates excess Ca^{2+} or other molecules from the mitochondrial matrix. Pathologic opening of mtPTP leads to excessive release of NADH/NAD^+, Krebs cycle intermediates, and other small solutes eventually inhibiting Krebs cycle and mitochondrial respiration (Zoratti and Szabo 1995). Increased levels of ROS

sensitize mtPTP opening to ionized calcium (Zoratti and Szabo 1995; Williams, Van Remmen et al. 1998). This mode of inhibition was proposed for *Sod2*$^{-/-}$ mice liver mitochondria, which resulted in loss of uncoupled respiration due to collapse of ΔΨ (Kokoszka, Coskun et al. 2001).

Results

Histochemical and structural abnormalities of Epas1$^{-/-}$ *mice*

A clinically useful marker for mitochondrial disease is the presence of ragged red fibers (RRFs), detected histologically using either a modified Gomori or succinate dehydrogenase (SDH) activity stain (Rifai, Welle et al. 1995). Appearance of RRF is due to clumps of abnormal mitochondria in the subsarcolemmal region of the muscle fiber. We showed that SDH activity is higher around the periphery and within skeletal muscle fibers of *Epas1*$^{-/-}$ mice (Figure 3-2a). Cytochrome oxidase (COX) staining is also stronger in both skeletal muscle and heart myofibers. Transcript levels of OXPHOS components including SDH and COX subunits are known to be upregulated in the affected tissues of mitochondrial disease patients, presumably as an attempt by the cells to compensate for the mitochondrial energetic defect (Munnich, Rotig et al. 1996; Wallace 2001). This finding suggests an OXPHOS defect in *Epas1*$^{-/-}$ mice.

Ultrastructural studies showed individual mitochondrial hypertrophy without hyperplasia, with the mitochondrial area fraction 50% greater in cardiac myocytes from *Epas1*$^{-/-}$ (66.0 ±7.5%) versus wild-type (42.1 ±2.7%) mice. Cardiac myocytes and hepatocytes from *Epas1*$^{-/-}$ mice contain degenerating

mitochondria with thinned and clarified matrix, but intact inner membrane (Figure 3-2b). Hepatocytes contain degenerating mitochondria, as well. However, mitochondrial area fraction (mitochondrial area/cytoplasmic area) and mitochondrial number are similar in skeletal muscle and liver.

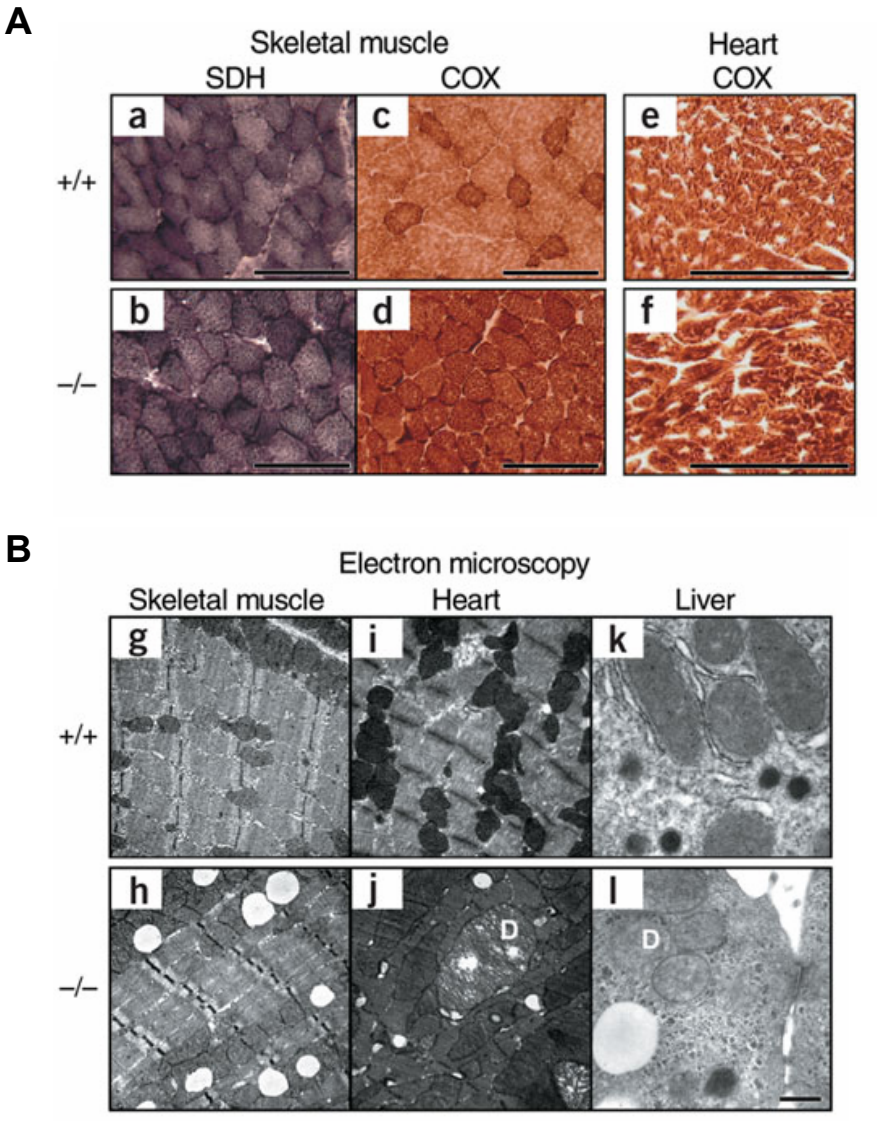

Figure 3-2. Histochemical and ultrastructural studies of mitochondria
A SDH and COX staining of skeletal muscle and COX staining of heart,
B Degenerating mitochondria (D) are present in heart and liver of *Epas1*$^{-/-}$ mice. Black bar represents 1 μm. *Adapted from (Scortegagna, Ding et al. 2003)*

Increased superoxide production in Epas1$^{-/-}$ liver

Biochemical and mitochondrial abnormalities observed in *Epas1*$^{-/-}$ mice are strikingly similar to *Sod2*$^{-/-}$ mice, which were shown to have mitochondrial ROS toxicity due to the absence of MnSOD. Therefore, possible involvement of ROS toxicity was investigated in *Epas1*$^{-/-}$ mouse liver mitochondria. Using two different methods, we observed increased SO levels in liver sections and increased production of SO by liver submitochondrial particles (SMPs) of *Epas1*$^{-/-}$ mice (Figure 3-3). Dihydroethidine (2′, 7′-dichlorofluorescin diacetate, DCFH-DA) is converted to its fluoregenic form, dichlorofluorescin, upon interaction with superoxide and is useful for qualitative analysis of SO levels. In Fig 3-3a, it is evident that there is increased fluorescence due to higher SO levels. Ferricytochrome c reduction is a more quantitative indicator of SO production. Liver SMPs were prepared from wild-type and *Epas1*$^{-/-}$ mouse liver (See Materials and Methods section for a detailed protocol) and as shown in Fig 3-3b, SMPs from *Epas1*$^{-/-}$ mouse liver exhibit three-fold higher rates of SO production. Therefore, we showed by two different assays that there is increased SO levels/production in *Epas1*$^{-/-}$ mouse liver mitochondria compared to wild-type.

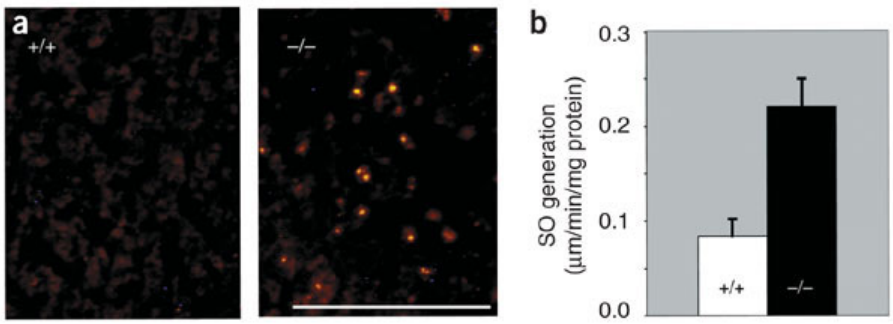

Figure 3-3. Increased SO production by *Epas1*$^{-/-}$ mouse liver mitochondria.
A Dihydroethidine staining of frozen liver sections of wild-type and Epas1$^{-/-}$ mice. Areas of extreme intensity have been aliased from red to yellow. The white bar represents 100 μm.
B SO generation rates by SMPs isolated from liver shows increased SO production by Epas1$^{-/-}$ mice compared to wild-type littermates. Error bars represent S.E.M, n=4, $p < 0.05$
Adapted from (Scortegagna, Ding et al. 2003)

Reduced levels of AOE genes in Epas1$^{-/-}$ mice

Increased ROS levels often precede the induction of major anti-oxidant enzyme (AOE) gene expression, including *Sod2, catalase, GPx1,* and *Sod1* (Fridovich 1999). However, real-time PCR analysis of liver AOE gene expression revealed reduced or unchanged mRNA levels of *Sod2, catalase, GPx1, and Sod1* in *Epas1*$^{-/-}$ mice compared to wild-type littermates (Figure 3-4a). Western-blot analysis of liver samples also showed lower MnSOD protein levels in *Epas1*$^{-/-}$ mice, compared to wild-type. This unexpected finding suggested a possible role for HIF-2α in regulation of AOE gene expression. However, induction of other stress-induced genes (e.g. Ddit3, Mt2) in *Epas1*$^{-/-}$ mice suggests that alternative pathways for oxidative stress are still active in the absence of HIF-2α.

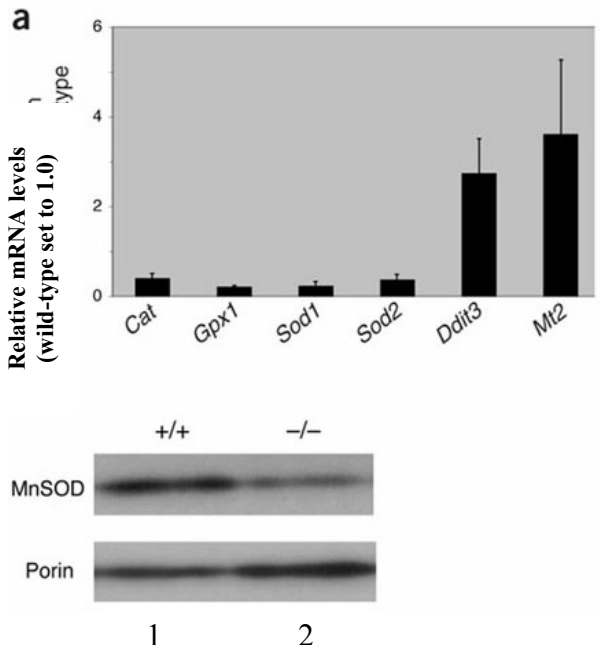

Figure 3-4. AOE gene expression reveals impaired AOE response in *Epas1*$^{-/-}$ liver.
A Reduced levels of major AOE gene transcripts in *Epas1*$^{-/-}$ mice
N=3-5 sets analyzed in triplicates, each set consists of two different RNA pools from three different mice.
Error bars represent S.E.M, $p < 0.05$
B Reduced protein levels of MnSOD/Sod2, compared to mitochondrial protein porin in *Epas1*$^{-/-}$ mice.
Adapted from (Scortegagna, Ding et al. 2003)

HIF-2α induces major AOE promoters

Reduced expression of major AOE genes despite higher SO levels in *Epas1*$^{-/-}$ mice suggested a possible role for HIF-2α in their transcriptional regulation. To test this hypothesis, promoter regions (~2 kb upstream of the transcriptional start site) of mouse *Sod2, Cas1, Gpx1* and *Sod1* genes were placed in luciferase reporter constructs. An HIF-2α expression plasmid was co-transfected with luciferase reporter constructs into HEK293 cells and luciferase activity was measured (Figure 3-5). All major AOE gene promoters are induced comparably to the positive-control reporter HRE-tk, by HIF-2α over-expression. A negative control, the Hsp90 promoter, is not induced significantly by HIF-2α. Co-transfection of ARNT with HIF-2α increased the fold-elevation (data not shown). HIF-1α was much less effective at inducing AOE promoters (data not shown). Further experiments are under way to determine the mechanism by which HIF-2α activates AOE promoters.

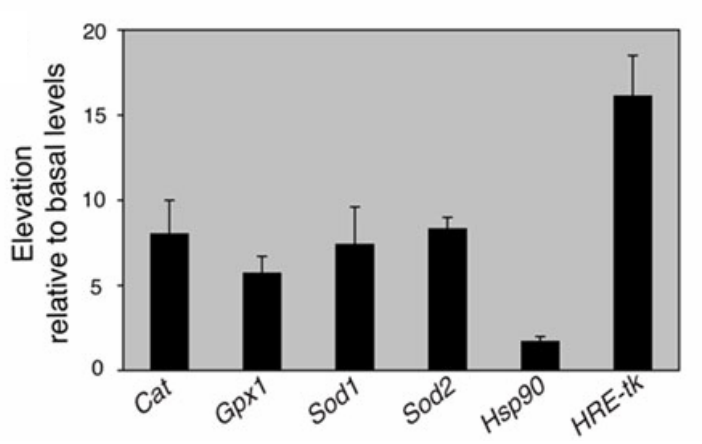

Figure 3-5. Major AOE gene promoters are induced by HIF-2α
Reporter constructs were co-transfected with or without (basal level) an HIF-2α expression vector into HEK293 cells and luciferase activity was measured. Error bars represent S.E.M., n=5 in quadruplicate
Adapted from (Scortegagna, Ding et al. 2003)

SOD mimetic reverses several aspects of Epas1$^{-/-}$ phenotype

In support of oxidative stress as an etiology for the *Epas1*$^{-/-}$ phenotype, treatment of newborn mice with a SOD mimetic, manganese III tetrakis (5,10,15,20 benzoic acid) or MnTBAP, showed recovery of many pathologies present in *Epas1*$^{-/-}$ mice. Relative to untreated *Epas1*$^{-/-}$ mice, *Epas1*$^{-/-}$ mice treated with MnTBAP showed a substantial correction of hypoglycemia (9.9 ±1.1 mmol l^{-1} in treated *Epas1*$^{-/-}$ mice versus 5.0 ±0.5 mmol l^{-1} in untreated *Epas1*$^{-/-}$ mice) and serum lactate levels (9.4 ±0.4 mmol l^{-1} in treated *Epas1*$^{-/-}$ mice versus 18.3 ±1.4 mmol l^{-1} in untreated *Epas1*$^{-/-}$ mice). These effects were not attributed to nonspecific effects of MnTBAP, as we observed no significant changes in serum levels of glucose (11.8 ±0.7 mmol l^{-1} in treated wild-type mice versus 12.4 ±0.6 mmol l^{-1} in untreated wild-type mice) or lactate (2.5 ±0.3 mmol l^{-1} in treated wild-type mice versus 3.3 ±0.2 mmol l^{-1} in untreated wild-type mice) in wild-type mice similarly treated with MnTBAP or left untreated. Also, *Epas1*$^{-/-}$ mice treated with MnTBAP had substantial fewer lipid deposits in the liver (Figure 3-6).

To determine if oxidative stress contributes to embryonic lethality, pregnant females carrying *Epas1*$^{-/-}$ embryos were treated with MnTBAP. Treatment of pregnant females with MnTBAP resulted in higher viability ratio for *Epas1*$^{-/-}$ mice, 18 % of total viable progeny, compared to untreated mice, 6 %. Interestingly, treatment of Sod2$^{-/-}$ mice with MnTBAP had been shown to reverse several pathologies in Sod2$^{-/-}$ mice (Melov, Schneider et al. 1998).

A

	Epas1+/+ untreated	Epas1+/+ treated	Epas1-/- untreated	Epas1-/- treated
Glucose (mM)	12.4 +/- 0.6	11.8 +/- 0.7	5.0 +/- 0.5	9.9 +/- 1.1
Lactate (mM)	3.3 +/- 0.2	2.5 +/- 0.3	18.3 +/- 1.4	9.4 +/- 0.4

B

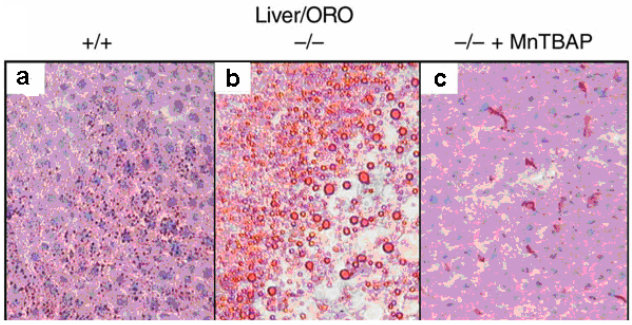

Figure 3-6. Reversal of hypoglycemia, lactate accumulation and lipid deposition in *Epas1*$^{-/-}$ liver by SOD mimetic
Newborn mice were treated daily with intraperitoneal injection of MnTBAP between postnatal days 3-28. ***A*** Serum glucose and lactate levels, ***B*** Liver sections from **a** Wild-type, **b** *Epas1*$^{-/-}$ untreated, ***c*** *Epas1*$^{-/-}$ treated mice were stained with oil Red O and images were obtained from 20x fields. *Adapted from (Scortegagna, Ding et al. 2003)*

The data presented so far suggest that oxidative stress plays a major role in pathologies observed in *Epas1*$^{-/-}$ mice. We were next interested in determining whether a specific defect in mitochondria function occurred in *Epas1*$^{-/-}$ mice.

Impaired respiration of Epas1$^{-/-}$ *liver mitochondria*

To determine the specific effect of the absence of HIF-2α on liver mitochondrial function, we analyzed respiration of isolated liver mitochondria using an oxygen polarography technique (Estabrook 1967). Isolated mitochondria were incubated in the presence of either: i) complex I-linked substrates (glutamate + malate, see Fig 3-1) that enter the TCA cycle and generate NADH to be oxidized by complex I, or ii) complex II-linked substrate succinate (in the presence of complex I inhibitor, rotenone). Succinate is oxidized by complex II (SDH) and electrons are transferred to $FADH_2$ instead of NADH.

Therefore, by using two different types of substrates that generate electrons in two different ways, we can differentiate defects specific to each pathway. The respiration rate in the presence of glutamate + malate or succinate is defined as "state II" rate. State II rate is limited by the availability of ADP. Upon addition of ADP, respiration rate increases dramatically due to ATP synthesis by complex V using the chemiosmotic gradient: The rate of oxygen consumption under these conditions is defined as "state III" rate. After all ADP is converted to ATP by complex V, respiration rate slows again due to limitation of electron flow by increased $\Delta\Psi$: "state IV" respiration. The ratio of state III to state IV is defined as the Respiratory Control Ratio (RCR) and is a measure of the coupling between electron transport and ATP generation by complex V.

State III and state IV respiration rates of isolated liver mitochondria were measured in the presence of glutamate + malate or succinate + rotenone (Figure 3-7). In the presence of glutamate + malate, *Epas1*$^{-/-}$ liver mitochondria exhibited lower state III rates compared to *Epas1*$^{+/+}$ liver mitochondria (31.8 ± 2.2 versus 39.9 ± 2.8 nmol atoms oxygen/min/mg-protein, p=0.050). In the presence of succinate, state III respiratory rates for *Epas1*$^{-/-}$ liver mitochondria trended slightly lower compared to *Epas1*$^{+/+}$ liver mitochondria, but the difference did not reach statistical significance. State IV respiratory rates were similar between *Epas1*$^{-/-}$ and *Epas1*$^{+/+}$ liver mitochondria with glutamate + malate or succinate as substrates. Lower state III and normal/higher state IV rates resulted in lower RCR values of *Epas1*$^{-/-}$ mitochondria. For glutamate + malate, there was a 25%

reduction in RCR (4.2 ± 0.3 versus 5.6 ± 0.9, p=0.020) and for succinate there was an 18 % reduction in RCR (3.3 ± 0.1 versus 4.1 ± 0.3, p=0.051).

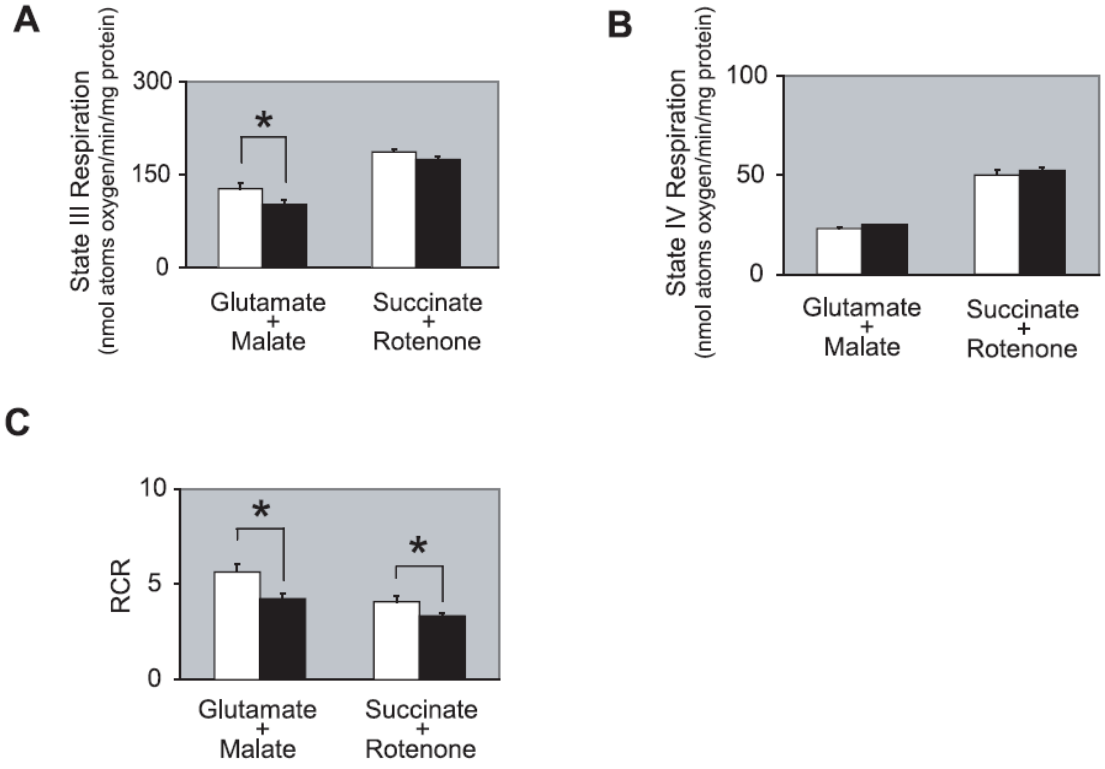

Figure 3-7. *Epas1*$^{-/-}$ liver mitochondria have impaired mitochondrial respiration. (a) State III respiration or (b) State IV respiration rates in the presence of Complex I-linked substrates (glutamate plus malate) or Complex II-linked substrate (succinate in the presence of rotenone). (c) Respiratory Control Ratio (RCR) for Complex I-linked substrates or Complex II-linked substrate. RCR is calculated as the ratio of State III to State IV respiratory rates (Estabrook 1967). Open bars represent *Epas1*$^{+/+}$ livers and solid bars represent *Epas1*$^{-/-}$ livers. Each value represents the mean ± S.E.M. of five different experiments. *P<0.05 by Student's t test (two-tailed).

ETC enzyme activities are preserved in Epas1$^{-/-}$ *liver*

A possible cause of reduced state III respiration and RCR is oxidative inactivation of one or more ETC enzyme complexes, especially those that

contain Fe-S centers, by ROS. Therefore we examined ETC enzyme activities (Figure 3-8). In contrast to the oxygen consumption data, individual ETC enzyme activities assessed under optimal, first order rate conditions were unchanged/or increased in *Epas1*$^{-/-}$ liver mitochondria (Fig 3-8a). NADH:ubiquinone reductase (NUR, Complex I) activity trended towards higher values in *Epas1*$^{-/-}$ mice compared to *Epas1*$^{+/+}$ liver mitochondria (191.9 ± 19.6 versus 147.5 ± 9.4 nmol/min/mg, p=0.533). Succinate dehydrogenase (SDH, Complex II) activity was upregulated in *Epas1*$^{-/-}$ compared to *Epas1*$^{+/+}$ liver mitochondria (209.3 ± 14.4 versus 148.8 ± 9.7 nmol/min/mg, p=0.004). However, ubiquinol:cytochrome c reductase (UCCR, Complex III) and cytochrome oxidase (COX, Complex IV) activities were not significantly different in *Epas1*$^{-/-}$ versus *Epas1*$^{+/+}$ liver mitochondria. Activity of citrate synthase (CS), a Krebs Cycle enzyme was increased in *Epas1*$^{-/-}$ versus *Epas1*$^{+/+}$ liver mitochondria (505 ± 28 versus 437 ± 16 nmol/min/mg, p=0.051).

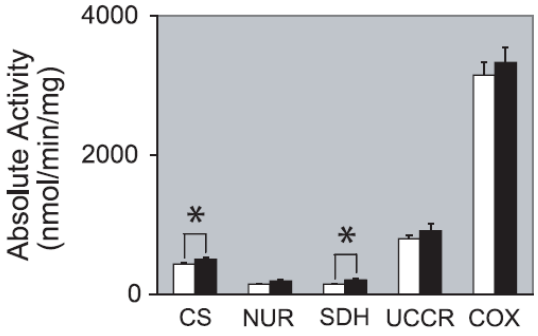

Figure 3-8. *Epas1*$^{-/-}$ liver mitochondria have preserved oxidative phosphorylation enzyme activities. (a) OXPHOS enzyme activities of citrate synthase (CS), NADH:ubiquinone reductase (NUR, Complex I), succinate dehydrogenase (SDH, Complex II), ubiquinol:cytochrome c reductase (UCCR, Complex III), or cytochrome oxidase (COX, Complex IV) using liver submitochondrial particles. Each value represents the mean ± S.E.M. of eight different experiments *P<0.05 by Student's t test (two-tailed).

Mitochondrial ATPase activity is increased in Epas1$^{-/-}$ liver

The ETC enzyme activity results indicate that ETC enzyme activities are not impaired by the increased oxidative stress state present in *Epas1*$^{-/-}$ liver mitochondria. Thus, the decreased state III respiration rates must be due to other factors that affect OXPHOS. One cause of reduced state III respiration in well-coupled mitochondria is impaired Complex V activity. To test for this possibility, mitochondrial ATPase activity was measured using submitochondrial particles (SMPs). SMPs from *Epas1*$^{-/-}$ liver mitochondria had higher ATPase activity (0.99 ± 0.04 versus 0.77 ± 0.05 μmol/min/mg, p=0.012), eliminating impaired Complex V activity as an etiology for lower state III respiration rates (Figure 3-9).

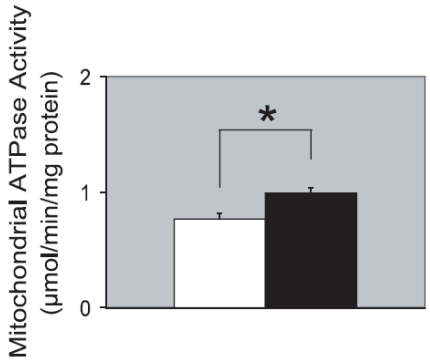

Figure 3-9. Mitochondrial ATPase activity.
Open bars represent *Epas1*$^{+/+}$ liver samples and solid bars represent *Epas1*$^{-/-}$ liver samples. Each value represents the mean ± S.E. of four different experiments. **P*<0.05 by Student's *t* test (two-tailed).

Sensitized *mtPTP opening in Epas1*$^{-/-}$ *liver mitochondria*

Altered membrane biophysical properties, including membrane potential and mitochondrial permeability transition pore (mtPTP) opening, may affect mitochondrial respiration. Therefore, we measured the mitochondrial membrane potential and mitochondrial permeability transition pore opening times for *Epas1*$^{-}$

$^{/-}$ liver mitochondria. Mitochondrial membrane potential revealed similar values for *Epas1*$^{-/-}$ and *Epas1*$^{+/+}$ liver mitochondria (Fig 3-10a) indicating *Epas1*$^{-/-}$ liver mitochondria have no inherent defects in membrane potential under basal conditions.

mtPTP opening is a biophysical property of mitochondria that is facilitated under physiological and pathophysiological stresses including oxidative stress. Hyper-sensitized opening of mtPTP may have adverse effects on mitochondrial respiration. To evaluate whether mtPTP was altered under basal conditions or with stimulation, we examined mtPTP opening in the absence or presence of ionized calcium (Ca^{2+}), respectively. In the absence of Ca^{2+}, there was no difference between *Epas1*$^{-/-}$ and *Epas1*$^{+/+}$ liver mitochondria mtPTP opening. However, in the presence of 250 μM Ca^{2+}, *Epas1*$^{-/-}$ liver mitochondria underwent more rapid mtPTP opening compared to *Epas1*$^{+/+}$ liver mitochondria (Fig 3-10b) indicating they are sensitized to conditions that induce mtPTP opening.

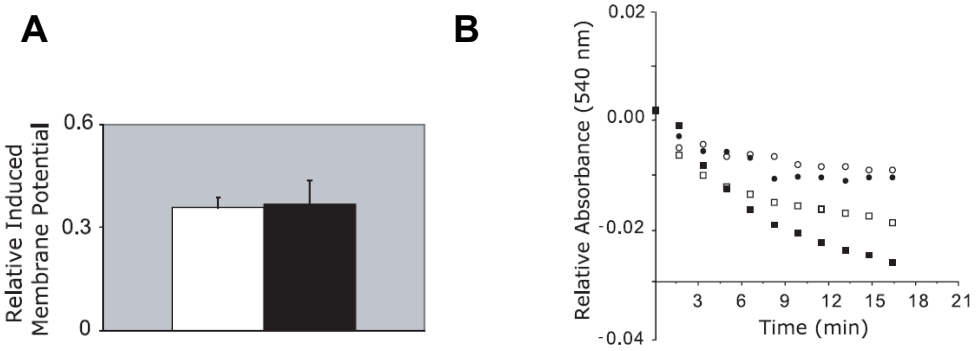

Figure 3 -10. *Epas1*$^{-/-}$ liver mitochondria have preserved mitochondrial membrane potential, but sensitized mitochondrial membrane permeability transition pore opening. ***A*** Mitochondrial membrane potential was measured using safranine. Open bars represent *Epas1*$^{+/+}$ liver samples and solid bars represent *Epas1*$^{-/-}$ liver samples ***B*** Mitochondrial membrane permeability transition pore opening times measured in the absence (circles) or presence (squares) of exogenous calcium for *Epas1*$^{+/+}$ mitochondria (open circles and squares) and *Epas1*$^{-/-}$ mitochondria (solid circles and squares). Shown is a representative tracing from one of four independent experiments.

Reduced mitochondrial aconitase activity in Epas1$^{-/-}$ liver

Although individual activity measurements of ETC complexes did not reveal any impairment in *Epas1*$^{-/-}$ liver mitochondria, it is possible that they can not coordinate or function together as efficiently as in wild-type mitochondria. Therefore, NADH oxidase activity of liver SMPs was measured. Because, NADH is the substrate and cytochrome c is the final electron acceptor in this assay, the activity does not depend on Krebs cycle activity, but depends on coordination between different complexes and ubiquinone. However, we found increased activity for *Epas1*$^{-/-}$ liver SMPs compared to wild-type controls (141.65 ± 14.47 versus 111.63 ± 10.04 nmol/min/mg, p=0.036),

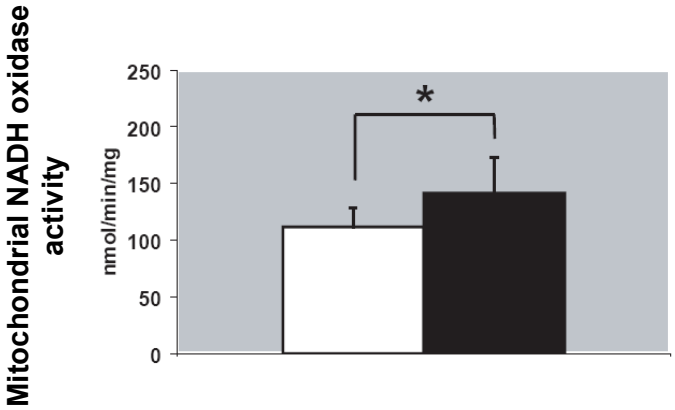

Figure 3-11. Mitochondrial NADH oxidase activity. NADH consumption by SMPs in the presence of cytochrome c was measured. Open bar represent *Epas1*$^{+/+}$ liver samples and solid bar represent *Epas1*$^{-/-}$ liver samples. Each value represents the mean ± S.E. of eight different experiments. **P*<0.05 by Student's *t* test (two-tailed).

Rather than a defect in ETC function, all these data point to a defect in Krebs cycle function that would selectively affect complex I-linked respiration. Therefore, activities of Krebs cycle enzymes aconitase, α-KGDH, and fumarase were measured. Aconitase is the most sensitive enzyme to ROS inactivation,

whereas fumarase is not sensitive. Measurement of aconitase activity in liver SMPs revealed ~ 20 % reduction in *Epas1*$^{-/-}$ compared to *Epas1*$^{+/+}$ liver mitochondria (200.65 ± 15.75 versus 254.02 ± 8.44 nmol/min/mg, p=0.025) (Figure 3-12a). Fumarase activity was not changed significantly (653.27 ± 51.37 versus 719.09 ± 28.54 nmol/min/mg, p=0.32), neither did α-KGDH, a less-sensitive enzyme to ROS (75.38 ± 9.71 versus 66.46 ± 5.14 nmol/min/mg, p=0.32). Tissue-specific Inhibition of aconitase is also observed in *Sod2-/-* mice (22-40% inhibition) (Li, Huang et al. 1995) and may explain the reduced state III rates in *Epas1*$^{-/-}$ mitochondria. Being the most sensitive oxidative stress marker of enzymatic proteins known, it is understable that its activity is partially reduced in *Epas1*$^{-/-}$ liver mitochondria.

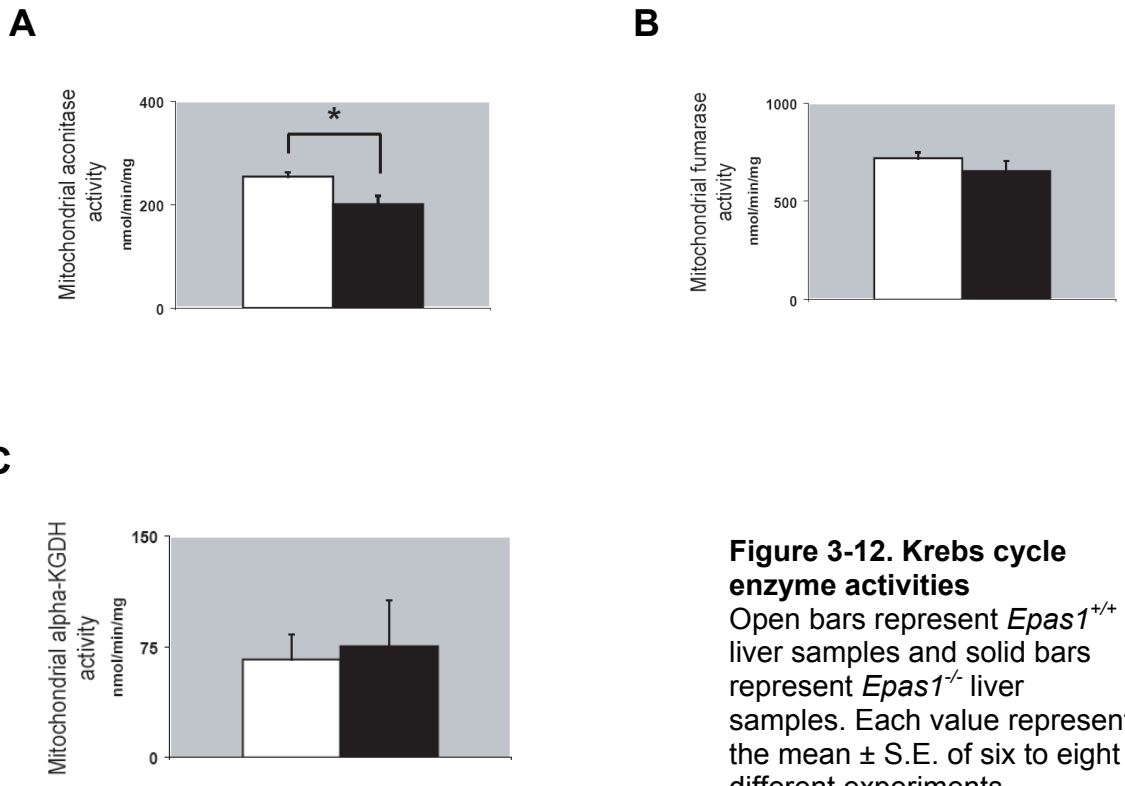

Figure 3-12. Krebs cycle enzyme activities
Open bars represent *Epas1*$^{+/+}$ liver samples and solid bars represent *Epas1*$^{-/-}$ liver samples. Each value represents the mean ± S.E. of six to eight different experiments.
**P*<0.05 by Student's *t* test (two-tailed).

Redox state of liver is altered in Epas1$^{-/-}$ mice

Mitochondrial disease states due to impaired OXPHOS are characterized by a more reduced cytoplasmic redox state (Munnich, Rotig et al. 1996). The NADH/ NAD^+ ratio reflects the cytoplasmic redox state (Veech, Eggleston et al. 1969) and is in equilibrium with lactate/pyruvate ratio. We determined lactate, pyruvate, and lactate/pyruvate ratio for *Epas1$^{-/-}$* liver using whole liver (cytosolic) perchloric acid (PCA) extracts (Figure 3-13). For *Epas1$^{-/-}$* compared to *Epas1$^{+/+}$* liver samples, we observed higher lactate concentration (5.8 ± 1.2 versus 1.9 ± 0.5 µmol/g, p=0.019), similar pyruvate concentration (0.24 ± 0.05 versus 0.20 ± 0.02 µmol/g), and an increased lactate/pyruvate ratio (34.3 ± 8.0 versus 11.3 ± 4.0, p=0.03).

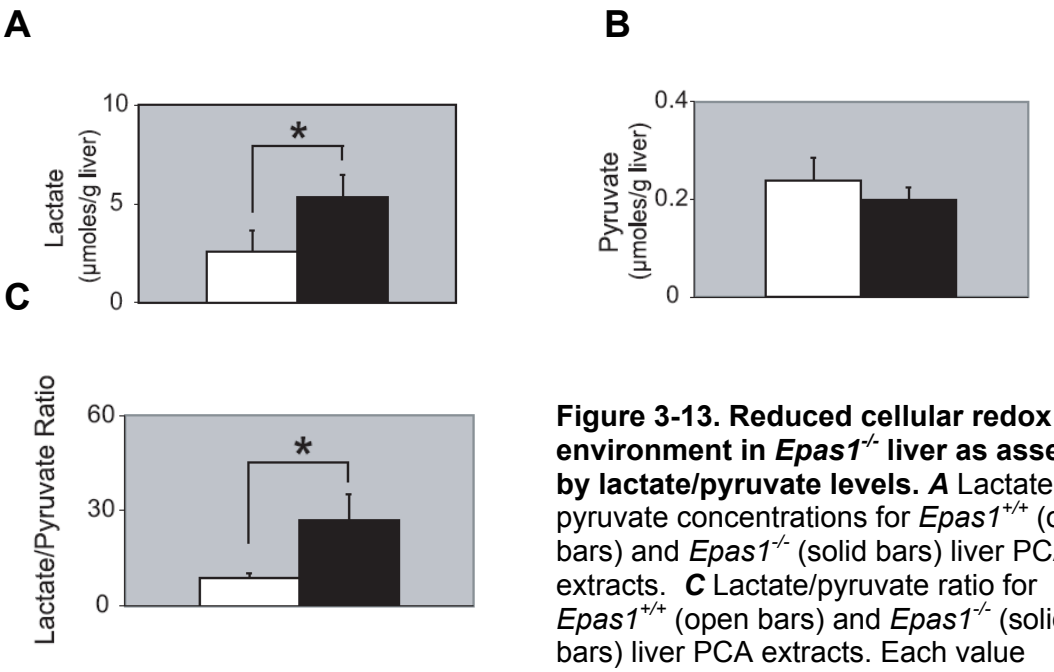

Figure 3-13. Reduced cellular redox environment in *Epas1$^{-/-}$* liver as assessed by lactate/pyruvate levels. ***A*** Lactate and ***B*** pyruvate concentrations for *Epas1$^{+/+}$* (open bars) and *Epas1$^{-/-}$* (solid bars) liver PCA extracts. ***C*** Lactate/pyruvate ratio for *Epas1$^{+/+}$* (open bars) and *Epas1$^{-/-}$* (solid bars) liver PCA extracts. Each value represents the mean ± S.E. of five different experiments. **P*<0.05 by Student's *t* test (two-tailed).

Reduced cellular redox state and lactate accumulation in *Epas1*$^{-/-}$ liver suggest increased glycolytic flux and increased conversion of pyruvate to lactate possibly to regenerate NAD^+ for glycolytic use.

Cytoplasmic redox states also affect the cellular GSH/GSSG ratio. Whole liver GSH levels, which reflect the cytosolic GSH levels given the size of the cytosolic GSH pool in comparison to the mitochondrial GSH pool, were not statistically different in *Epas1*$^{-/-}$ compared to *Epas1*$^{+/+}$ liver (3.2 ± 0.6 versus 4.0 ± 0.8 µmol/g) (Figure 3-14a) whereas whole liver GSSG levels were lower in *Epas1*$^{-/-}$ compared to *Epas1*$^{+/+}$ liver (0.04 ± 0.01 versus 0.06 ± 0.01 µmol/g, p=0.011) (Figure 3-14b). This resulted in a trend towards increased whole liver GSH/GSSG ratio for *Epas1*$^{-/-}$ versus *Epas1*$^{+/+}$ liver (172.8 ± 71.3 versus 69.4 ± 15.9, p=0.178) (Figure 3-14c).

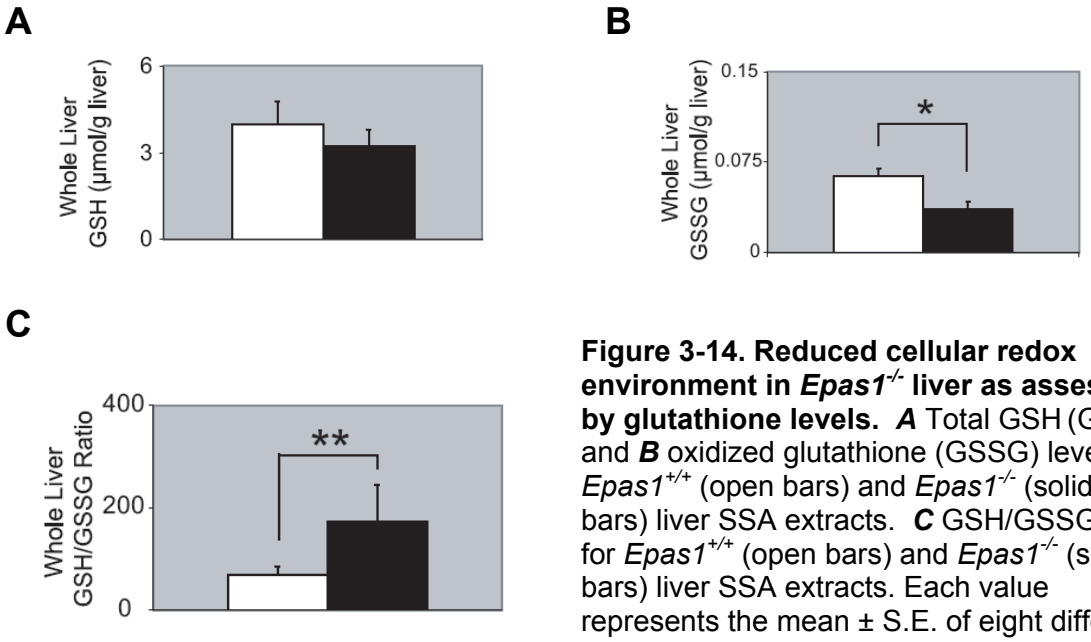

Figure 3-14. Reduced cellular redox environment in *Epas1*$^{-/-}$ liver as assessed by glutathione levels. ***A*** Total GSH (GSH) and ***B*** oxidized glutathione (GSSG) levels for *Epas1*$^{+/+}$ (open bars) and *Epas1*$^{-/-}$ (solid bars) liver SSA extracts. ***C*** GSH/GSSG ratio for *Epas1*$^{+/+}$ (open bars) and *Epas1*$^{-/-}$ (solid bars) liver SSA extracts. Each value represents the mean ± S.E. of eight different experiments. **P*<0.05, ***P*<0.2 by Student's *t* test (two-tailed).

On the other hand, mitochondrial GSH levels are determined by import rates from the cytoplasm and utilization rates within the mitochondria. Differences in mitochondrial GSH, GSSG, or GSH/GSSG ratios may be a consequence of increased oxidative stress states. Comparing *Epas1*$^{-/-}$ to *Epas1*$^{+/+}$ liver mitochondria, *Epas1*$^{-/-}$ liver mitochondria tended to have higher GSH levels (11.0 ± 2.8 versus 6.0 ± 0.8 µmol/gm protein, p=0.117) (Figure 3-15a). GSSG levels also trended higher in *Epas1*$^{-/-}$ liver mitochondria, although not to statistically significant levels (0.33 ± 0.11 versus 0.19 ± 0.03 µmol/gm protein, p=0.239) (Figure 3-15b). GSH/GSSG ratios were similar between the two groups (Figure 3-15c).

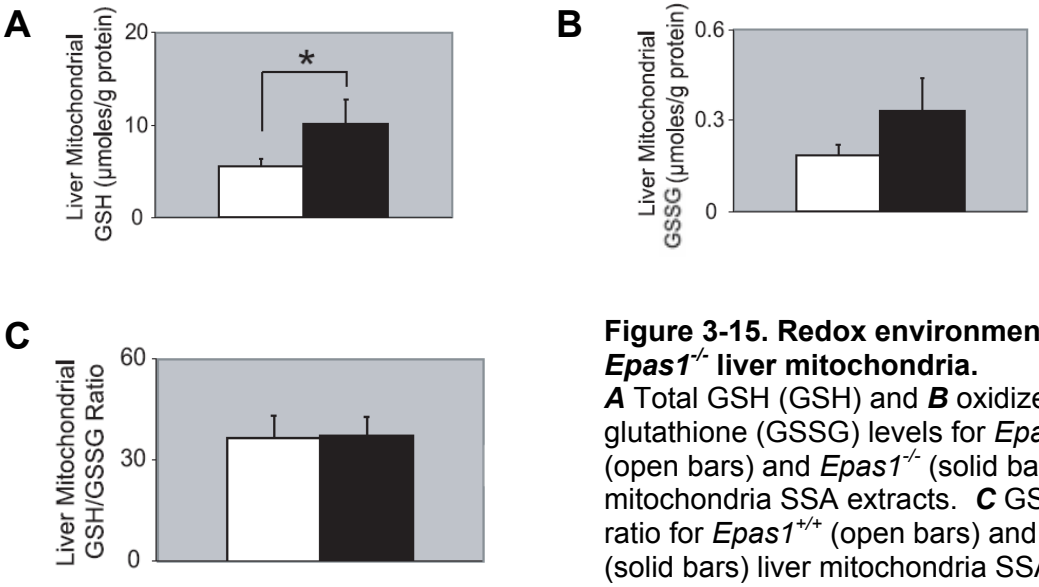

Figure 3-15. Redox environment in *Epas1*$^{-/-}$ liver mitochondria.
A Total GSH (GSH) and ***B*** oxidized glutathione (GSSG) levels for *Epas1*$^{+/+}$ (open bars) and *Epas1*$^{-/-}$ (solid bars) liver mitochondria SSA extracts. ***C*** GSH/GSSG ratio for *Epas1*$^{+/+}$ (open bars) and *Epas1*$^{-/-}$ (solid bars) liver mitochondria SSA extracts. Each value represents the mean ± S.E. of six different experiments. **P*=0.12 by Student's *t* test (two-tailed).

Although, the ratio of reduced to oxidized GSH is not different between *Epas1*$^{-/-}$ and wild-type mice, compared to their respective cytoplasm, *Epas1*$^{-/-}$

mitochondria are more oxidized. Increased amount of total GSH in *Epas1*$^{-/-}$ mitochondria may be due to increased import of it from the cytoplasm due to increased SO production.

Discussion

Studies of HIF-1α in the past decade have delineated a hypoxic response pathway in which HIF-1 serves as a master regulator of angiogenesis, glycolysis, glucose uptake, cell survival, and apoptosis. Although HIF-2α is structurally similar to HIF-1α, several lines of evidence indicate unique roles for HIF-2α. Our studies of *Epas1*$^{-/-}$ mice revealed an *in vivo* role for HIF-2α in the induction of major AOE gene expression in response to increased ROS production. In the absence of HIF-2α, an increased oxidative stress state and an ensuing mitochondrial disease results. The pathological similarities between *Epas1*$^{-/-}$ and *Sod2*$^{-/-}$ mice suggested inhibition of mitochondrial function as a common link. Our studies were aimed at defining the effect of the HIF-2α null mutation upon mitochondrial function in the liver, a prominent site of pathology for *Epas1*$^{-/-}$ mice.

Oxygen consumption measurements were performed to evaluate the effect of the HIF-2α mutation upon state III and state IV respiration. State III respiratory rate indicates the rate of oxygen consumption in the presence of substrate and ADP, whereas state IV respiration is measured after all ADP is consumed. Oxygen consumption measurements of coupled mitochondria from *Epas1*$^{-/-}$ mouse liver revealed lower state III respiration rates for complex I-linked

substrates and lower RCRs for both complex I- as well as complex II-linked substrates. State IV respiration rates of mitochondria isolated from *Epas1*$^{+/+}$ and *Epas1*$^{-/-}$ liver were unaffected, suggesting integrity of the mitochondrial inner membrane. A similar pattern of mitochondrial respiration inhibition was observed in *Sod2*$^{+/-}$ mouse liver (Williams, Van Remmen et al. 1998).

Respiration of complex I substrates is preferentially affected by inhibition of the Krebs Cycle whereas respiration of both complexes I and II are equally affected by ETC disorders downstream of complex III or by causes of OXPHOS deficiency that indirectly affect ETC function. The fuel substrate mixture glutamate + malate, when metabolized by the Krebs cycle, produces NADH which subsequently donates electrons to the ETC at complex I. The fuel substrate succinate is directly oxidized by succinate dehydrogenase (complex II) to form $FADH_2$ which subsequently transfers electrons to the ubiquinone pool. The reduced RCRs in *Epas1*$^{-/-}$ liver mitochondria for both complex I- and complex II-linked substrates indicate a general deficiency in OXPHOS function. The greater reduction of state III rates for glutamate + malate as opposed to succinate are consistent with an impairment in Krebs cycle function, such as aconitase inhibition. Therefore, the impairment in mitochondrial respiratory function in *Epas1*$^{-/-}$ liver mitochondria may involve deficiencies in both OXPHOS as well as Krebs cycle function.

Assessment of individual ETC enzyme activities and mitochondrial NADH oxidase activity indicated that the level of oxidative stress present in *Epas1*$^{-/-}$ liver did not result in damage to the ETC components. However, measurement of

oxygen consumption of isolated mitochondria provide a more physiologically relevant study of mitochondrial function (Lee 1995; Munnich, Rotig et al. 1996) as well as a more integrative index of metabolic capacity (Matecki, Py et al. 2002). Polarographic oxygen consumption studies of isolated coupled mitochondria not only detect ETC disorders, but also deficiencies of Krebs cycle enzymes, pyruvate dehydrogenase, shuttles/carriers, and substrates/co-factors.

As with the ETC, inhibition of the Krebs cycle can be direct or indirect. For example, direct inhibition may be a consequence of oxidative stress-induced damage to Krebs cycle enzymes. Increased ROS production in mitochondria can lead to reversible inhibition of mitochondrial aconitase by conversion of its [4Fe-4S] center to a [3Fe-4S] center due to removal of a labile iron (Drapier and Hibbs 1986; Nulton-Persson and Szweda 2001). α-ketoglutarate dehydrogenase (α-KGDH) (Tretter and Adam-Vizi 2000; Nulton-Persson and Szweda 2001; Nulton-Persson, Starke et al. 2003) and SDH (Nulton-Persson and Szweda 2001) are also other ROS-sensitive enzymes of the Krebs cycle. Of these enzymes, aconitase has been proposed as a sensitive marker of mitochondrial oxidative stress. Inhibition of aconitase is faster than complex-I or complex-II (Drapier and Hibbs 1986).In *Epas1*$^{-/-}$ liver mitochondria, we observed a 20 % reduction in aconitase activity of *Epas1*$^{-/-}$ liver mitochondria, whereas other enzymes that are less sensitive to ROS (i.e. fumarase, α-KGDH) were not impaired. Inhibition of aconitase may provide a possible explanation for reduced state III respiration of *Epas1*$^{-/-}$ liver mitochondria.

The elevated hepatic lactate levels and lactate/pyruvate ratio of *Epas1*$^{-/-}$ mice indicate an increased NADH/NAD^{+} ratio and a more reduced cytoplasmic redox state, a biochemical state commonly seen in mitochondrial myopathies (Munnich, Rotig et al. 1996; Graham, Waymire et al. 1997). Besides defects in ETC and OXPHOS coupling, indirect inhibition of the Krebs cycle may be a consequence of any scenario that reduces NAD^{+} levels. On the other hand, an increased mitochondrial NADH/NAD^{+} ratio can also occur via defects in NADH/NAD^{+} shuttles, increased loss of mitochondrial NAD^{+} stores by disruption of mitochondrial permeability or by increased mitochondrial to cytoplasmic flux due to increased NAD^{+} utilization.

The Mitochondrial Permeability Transition Pore (mtPTP) is a large complex composed of the inner membrane Adenine Nucleotide Translocase (ANT), outer membrane Voltage-Dependent Anion Channel (VDAC), Bax, Bcl-2, cyclophilin D, and benzadiazopine receptor (Zoratti and Szabo 1995; Wallace 2001). Physiological opening of mtPTP eliminates excess Ca^{2+} or other molecules from the mitochondrial matrix. Pathologic opening of mtPTP leads to excessive release of NADH/ NAD^{+}, Krebs cycle intermediates, and other small solutes eventually inhibiting Krebs cycle and mitochondrial respiration (Zoratti and Szabo 1995). Increased levels of ROS sensitize mtPTP opening to ionized calcium, similar to that observed for *Epas1*$^{-/-}$ liver mitochondria (Zoratti and Szabo 1995; Williams, Van Remmen et al. 1998). This mode of inhibition was also proposed for Sod2$^{-/-}$ mice liver mitochondria, which resulted in reduced state

III respiration and loss of uncoupling while state IV respiration remained unaffected (Kokoszka, Coskun et al. 2001).

Increased consumption of NAD^+ also results in increased $NADH/NAD^+$ ratios and Krebs cycle inhibition. During glycolysis, there is increased consumption of oxidized equivalents (NAD^+) as well as less efficient regeneration of NAD^+ when pyruvate, the end product of glycolysis, is converted to lactate in the cytoplasm. NADH generated in the cytoplasm from glycolysis is normally transported to mitochondria for oxidation back to NAD^+. As a result, the cytoplasmic $NADH/ NAD^+$ ratio is increased during glycolysis and the mitochondrial $NADH/NAD^+$ ratio may increase secondarily. Thus, the altered $NADH/NAD^+$ ratios in *Epas1*$^{-/-}$ liver samples may be due to a combination of ineffective OXPHOS action, impaired Krebs cycle function, and/or increased glycolytic energy metabolism.

The $NAD(P)H/NAD(P)^+$ redox couple is linked to the redox state in cells as well as mitochondria; the redox state is also influenced by the GSH/GSSG ratio, another important redox couple (Schafer and Buettner 2001). The redox environment is the description of the overall effect of the linked sets of redox couples (Schafer and Buettner 2001). The $NADH/NAD^+$ ratio, as demonstrated by the lactate/pyruvate ratio, indicates a potentially increased reductive state in *Epas1*$^{-/-}$ liver. In *Epas1*$^{-/-}$ liver, this occurred in a setting of elevated whole cell GSH/GSSG ratios, also consistent with a reductive state. Although the redox environment was not specifically measured, the data from these experiments

suggest an absence of cytoplasmic oxidative stress in *Epas1*$^{-/-}$ liver; rather, a reductive stress seems likely in *Epas1*$^{-/-}$ liver.

The GSH/GSSG redox couple is believed to be the main cellular redox buffer due to the very large size of reducing equivalents. Total GSH and GSH/GSSG ratios may or may not be altered in oxidative stress states (Van Remmen, Salvador et al. 1999; Schafer and Buettner 2001), depending upon the ability of cells to regenerate glutathione stores. Oxidative stress induces the formation of GSSG, potentially at the expense of GSH. To maintain a favorable redox environment, cells subjected to oxidative stress can increase the export of GSSG, thereby normalizing oxidative stress or even inducing a reductive stress (Sies and Akerboom 1984). The increase in the whole cell GSH/GSSG ratio for *Epas1*$^{-/-}$ liver is due to a decrease in GSSG levels; GSH levels for *Epas1*$^{-/-}$ liver are not significantly changed relative to *Epas1*$^{+/+}$ liver. Thus, the reductive environment in *Epas1*$^{-/-}$ liver may in part be the consequence of a compensatory response to increased oxidative stress.

Mitochondria are devoid of an ability to synthesize GSH; hence, mitochondrial GSH levels are dependent upon the activity of a GSH transporter (Griffith and Meister 1985; Fernandez-Checa, Kaplowitz et al. 1997). Inhibition of the GSH transporter by chronic alcohol consumption leads to increased ROS production by mitochondria, underscoring the importance of GSH as an important antioxidant in mitochondria. Thus, mitochondria effectively have a compartment-specific GSH pool that may be altered by the redox and/or oxidative state within

the mitochondria as well as by altered transport mechanisms. However, we have not measured the activity of this transporter in *Epas1*$^{-/-}$ liver mitochondria.

Relative to *Epas1*$^{+/+}$ liver mitochondria, *Epas1*$^{-/-}$ liver mitochondrial GSH and GSSG levels increased while the GSH/GSSG ratio remained unchanged. The increased total mitochondrial GSH concentration in *Epas1*$^{-/-}$ liver mitochondria implies that more GSH is imported into mitochondria from the cytosol. Despite the increase in GSH, the unchanged mitochondrial GSH/GSSG ratio indicates a substantial portion of the increased GSH is oxidized to GSSG in mitochondria. Hence, the increase in mitochondrial GSH levels in *Epas1*$^{-/-}$ liver mitochondria may alleviate, via an increase in redox buffering capacity (Schafer and Buettner 2001), oxidative stress caused by increased mitochondrial superoxide production in *Epas1*$^{-/-}$ liver (Scortegagna, Ding et al. 2003).

The data presented in these studies indicates HIF-2α is required for normal mitochondrial function. In the absence of HIF-2α, *Epas1*$^{-/-}$ mice have elevated lactate levels, dysregulated Krebs cycle intermediates, and defects in fatty acid oxidation consistent with generalized mitochondrial dysfunction (Scortegagna, Ding et al. 2003). The liver mitochondrial respiration studies support impaired Krebs cycle and/or OXPHOS function for *Epas1*$^{-/-}$ liver mitochondria. Inhibition of Krebs cycle and OXPHOS function may result in reduced mitochondrial ATP production. However, whole liver ATP levels were slightly decreased in *Epas1*$^{-/-}$ mice liver (data not shown), suggesting that glycolytic ATP production may have largely compensated for reduced mitochondrial ATP production. It is not known whether glycolytic metabolism

would satisfy the increased ATP demand if *Epas1*$^{-/-}$ mice were subjected to exercise, cold environment or other ATP-consuming stresses.

The role of HIF-2α in mitochondrial biology includes induction of antioxidant enzyme defenses to maintain mitochondrial ROS homeostasis. The ability of HIF members to respond to mitochondrial-generated ROS links HIF signaling to intermediary metabolism (Kietzmann and Gorlach 2005). In addition, Krebs cycle metabolites may also modulate the activity of HIF factors in a prolyl hydroxylase-dependent manner (Pollard, Briere et al. 2005; Selak, Armour et al. 2005; Wenger, Stiehl et al. 2005). Localization of members of the prolyl hydroxylase family that modulate HIF activity to the cytosol provides another possible link to intermediary metabolism that may depend directly upon mitochondrial substrate availability and function (Huang, Zhao et al. 2002; Metzen, Berchner-Pfannschmidt et al. 2003). Finally, lactate and pyruvate may also modulate HIF activity directly and as such would couple glycolytic metabolism to HIF activation (Lu, Forbes et al. 2002). Whether HIF-2α directly responds to other metabolites of intermediary metabolism remains the topic of future investigations.

CHAPTER FOUR

PROMOTER ANALYSIS OF MOUSE SOD2 GENE AND ITS REGULATION BY HIF-2α

Introduction

The mouse *Sod2* gene is located on chromosome 17 and is a single-copy gene. It contains five exons and four introns, similar to its human homolog. *Sod2* transcription is increased in response to increased oxidative stress, alcohol, cytokines and other stress-related stimuli (Porntadavity, Xu et al. 2001; St Clair 2004). Although human *Sod2* gene regulation has been well-studied, mouse *Sod2* regulation at the transcriptional level has not been examined in significant detail (Zhu, Huang et al. 2001; St Clair 2004). Both mouse and human promoters are TATA-less and human *Sod2* gene includes an intronic enhancer that modulates *Sod2* gene expression (Meyrick and Magnuson 1994; St Clair 2004). GC-rich sequences immediately upstream of transcriptional start site of mouse, bovine, and human *Sod2* gene contain Sp1 and AP-2 consensus sequences, which had suggested a role for Sp1 and AP-2 in its regulation (Figure 4-1). Subsequent studies of human *Sod2* basal promoter by site-directed mutagenesis showed that Sp1 is essential and sufficient for its expression (St Clair 2004). On the other hand, AP-2 has a negative effect on human *Sod2* gene expression through interaction with Sp1 (Zhu, Huang et al. 2001). Binding of Sp1 and AP-2 to human *Sod2* basal promoter leads to formation of a DNA loop structure, which

recruits transcription factors and co-activators (Mastrangelo, Courey et al. 1991). Further studies identified Egr-1, the early growth response

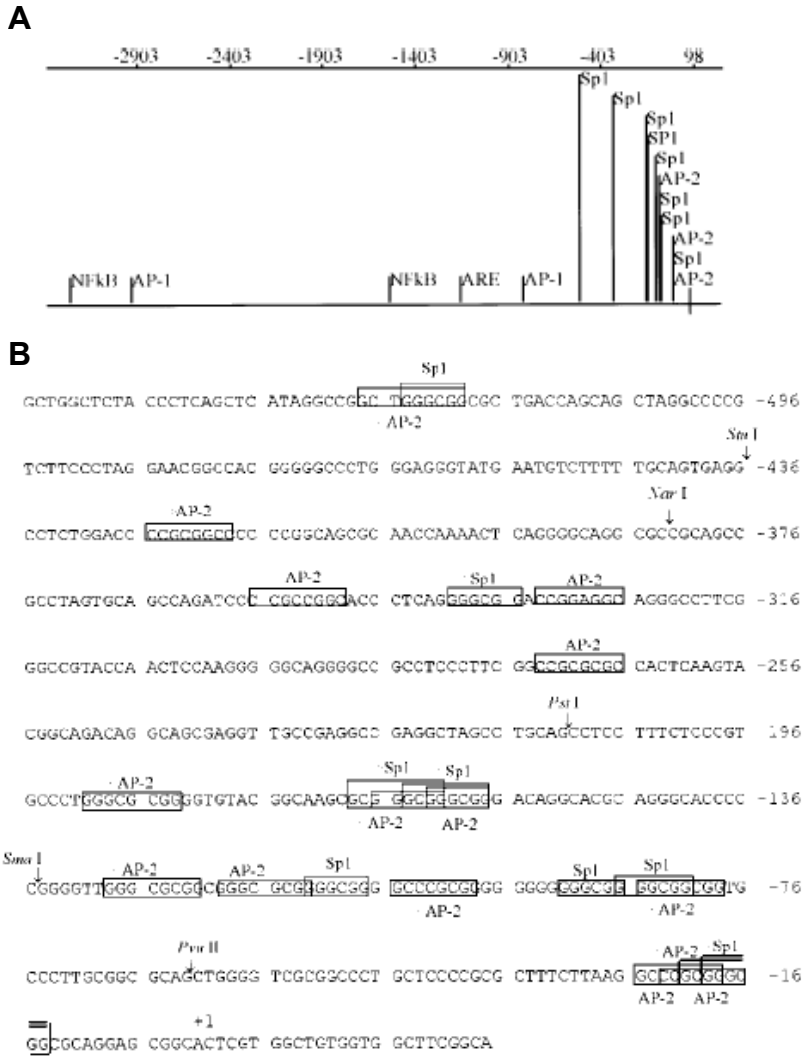

Figure 4-1. Human Sod2 promoter contains multiple Sp1 and AP-2 binding sites.
A Most transcription factor binding sites are located between -500 and +98 of Sod2 promoter.
B The region immediately upstream of transcriptional start site is GC-rich and contains multiple Sp1 and AP-2 consensus binding sites.
AP1: Activator protein 1, ARE: Anti-oxidant response element, NF-κB: Nuclear factor kappa-B
Adapted from (Xu, Porntadavity et al. 2002)

protein, as a negative regulator of human Sod2 transcription. However, its over-expression did not affect 12-O-tetradecanoylphorbol-13-acetate (TPA) - mediated upregulation of *Sod2* transcription (Porntadavity, Xu et al. 2001).

The enhancer regions within the second intron of both mouse and human *Sod2* genes contain binding sites for transcription factors (i.e. NF-κB, C/EBP, and nuclear factor-1) that mediate upregulation of *Sod2* transcription in response to TNF-α and IL-1β (Dhar, Lynn et al. 2004). However, the region responsible for transcriptional upregulation of *Sod2* in response to increased oxidative stress is not clearly identified yet.

Forkhead transcription factor FOXO3a/FKHRL1 has been shown to regulate transcription of *Sod2* gene under oxidative-stress conditions in quiescent colon carcinoma cells and mouse embryonic fibroblasts (Kops, Dansen et al. 2002; Nemoto and Finkel 2002). However, a recent study suggested that in HeLa cells, *Sod2* expression upon increased ROS does not require functional FOXO3a, whereas increased NF-κB activity due to serine/threonine protein kinase D (PKD) mediated phosphorylation was indispensable (Storz, Doppler et al. 2005). Therefore, various transcription factors may regulate *Sod2* expression depending on the cell-type and stimuli.

Impaired AOE gene response in *Epas1*$^{-/-}$ mouse liver and induction of *Sod2* promoter by HIF-2α in cell culture studies suggested that HIF-2α may mediate upregulation of *Sod2* transcription in response to increased SO production. After showing that mouse *Sod2* gene promoter between nucleotides -

1452 and +40 (relative to the transcriptional start site) is induced by HIF-2α, we aimed to identify the minimal region responsible for this regulation.

Results

Deletion analysis of mouse Sod2 (mSod2) promoter

We started analysis of mouse *Sod2* promoter by creating a series of 5' deletions fused to luciferase gene and tested their induction by HIF-2α or FOXO3a-A3, a constitutively active mutant FOXO3a that has all three sites of Akt phosphorylation mutated to alanine, in HEK293 cell line (Figure 1). Deletion of the region between -1452 and -553 led to a modest (30%) decrease in upregulation of *Sod2* promoter by HIF-2α, whereas it had a less dramatic effect on upregulation by FOXO3a-A3. However, HIF-2α is a more potent inducer of the mouse *Sod2* promoter, even after deletion of nucleotides between -1452 and -177. A step-like reduction in HIF-2α effect on mouse *Sod2* promoter suggests presence of regulatory sites throughout this region that interacts with HIF-2α, whereas FOXO3a-A3 shows a different mode of regulation.

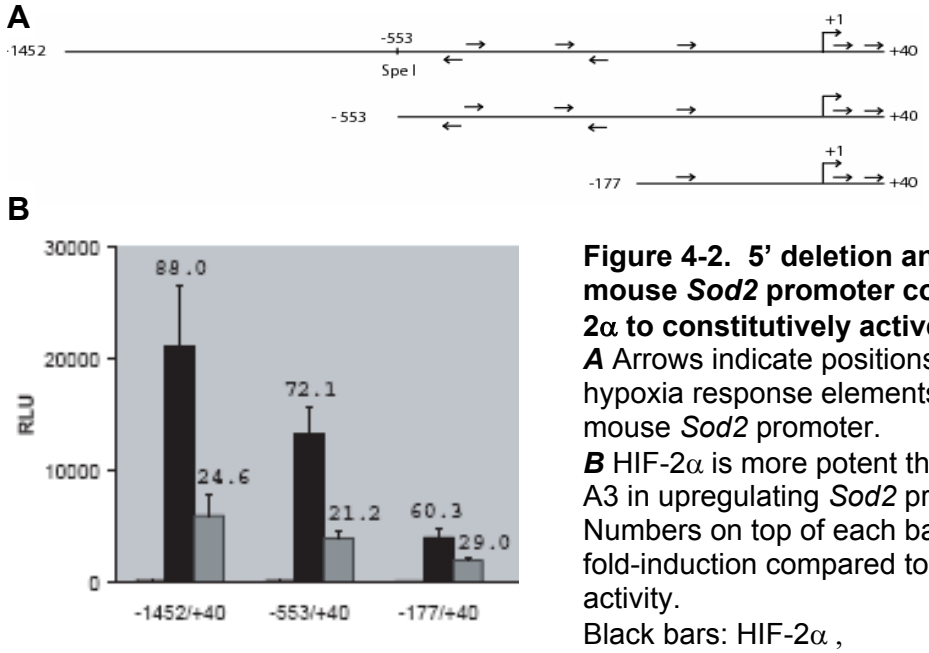

Figure 4-2. 5' deletion analysis of mouse *Sod2* promoter comparing HIF-2α to constitutively active FOXO3a-A3
A Arrows indicate positions of consensus hypoxia response elements (HREs) in mouse *Sod2* promoter.
B HIF-2α is more potent than FOXO3a-A3 in upregulating *Sod2* promoter. Numbers on top of each bar represents fold-induction compared to reporter alone activity.
Black bars: HIF-2α ,
Grey bars: FOXO3a-A3

Mutational analysis of HRE sites in mSod2 promoter

Importantly, -553/+40 construct contains all putative hypoxia response elements (HREs, usually described as "RCGTG") and retains 70% of activity. Therefore, we mutated all HREs upstream of "+1" and compared it to wild-type -553/+40 construct (Figure 4-3). Although we observed a substantial (44%) decrease in promoter activity, the mutant promoter (HRE1-5) was still inducible by HIF-2α, even more than by FOXO3a-A3. This suggests that HREs are necessary for full induction of *Sod2* promoter by HIF-2α, but they are not enough.

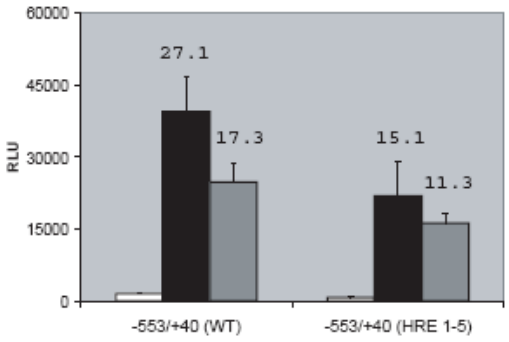

Figure 4-3. All HREs upstream of +1 of *Sod2* promoter were mutated, comparing HIF-2α to constitutively active FOXO3a-A3. HIF-2α can still induce *Sod2* promoter with all HREs mutated. Numbers on top of each bar represents fold-induction compared to reporter alone activity. Black bars: HIF-2α , Grey bars: FOXO3a-A3

Identification of evolutionarily conserved mSod2 promoter region

In order to find the conserved regions within the mouse *Sod2* promoter, we used a combination of different alignment programs such as DiAlign (http://www. genomatix.de), DiAlign + CHAOS (http://dialign.gobics.de/chaos-dialign-submission) and T-Coffee (http://www.ch.embnet.org/software/TCoffee .html). Figure 4-4 shows alignment of *Sod2* promoters from mouse, rat, dog,

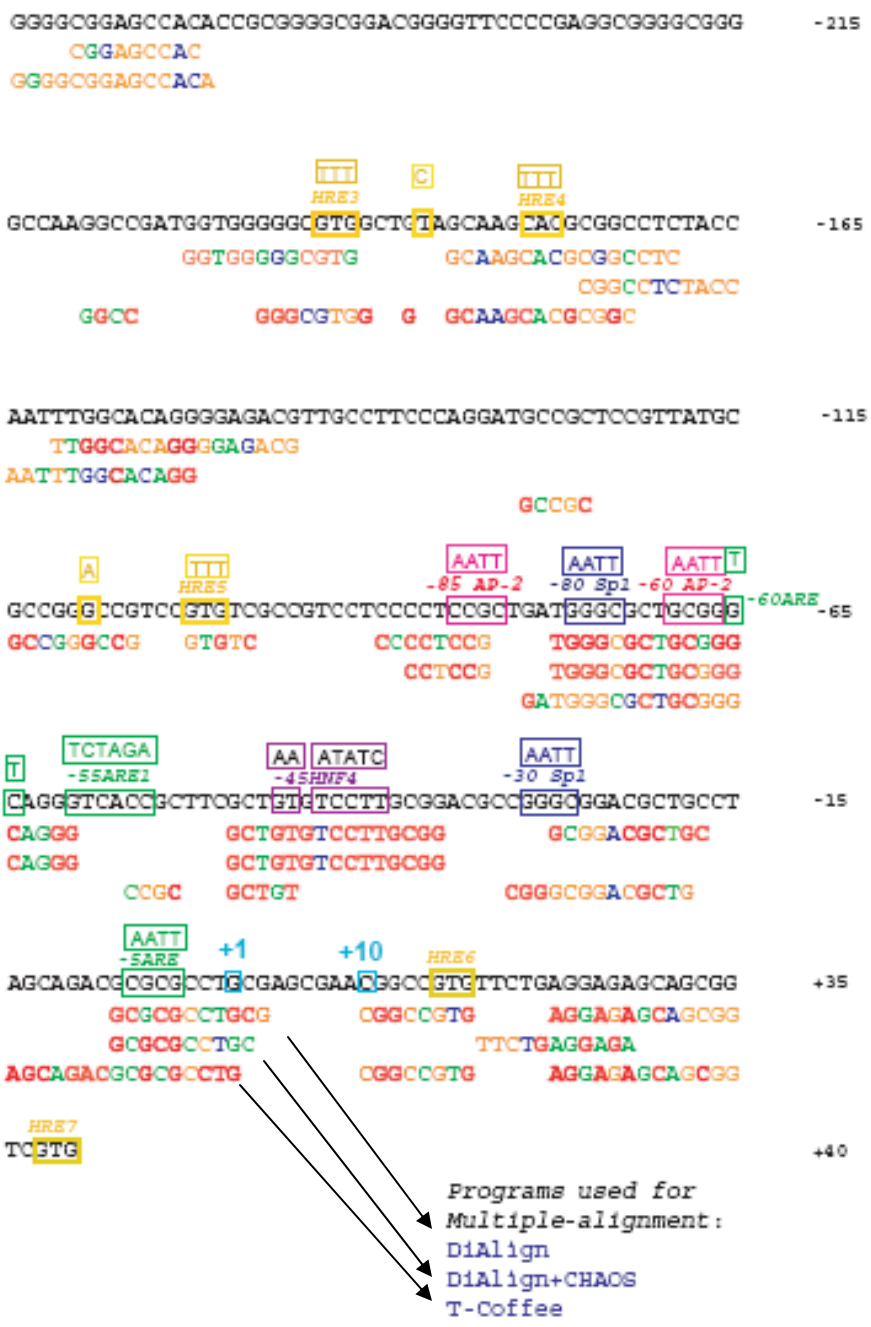

Figure 4-4. Multiple alignment of Sod2 promoter regions.
Mouse sequence (-265/+40) is shown in black letters. The first line shows aligned sequence by DiAlign, the second line shows DiAlign+CHAOS, and third line shows T-Coffee. Color coding was used to indicate conservation level: Red: 5/5 species, Orange: 4/5 species, Green: 3/5 species, Blue: 2/5 species.
Transcription factor binding sites were identified both using DiAlignTF and manually. Mutations are shown in boxes on top of each site.
Only the more significantly conserved region is shown.

chimp and human with conserved transcription factor sites and HREs marked. Mouse (Mus *musculus*) promoter (-960/+40) was used to retrieve *Sod2* promoter region sequences of rat (Rattus *norvegicus*), dog (Canis *familiaris*), chimp (Pan *troglodytes*) and human (Homo *sapiens*) from the Ensembl Database (www.ensembl.org).

By using this bioinformatics approach, we concluded that the region between -310 and +10 of mouse *Sod2* promoter is conserved and may contain the most important regulatory sites (Fig 4-4). To test this hypothesis, we compared -553/+40 to -310/+10 construct (Figure 4-5). Both HIF-2α and FOXO3a-A3 efficiently induced -310/+10 region, comparable to -553/+40 region. Therefore, we decided to focus on -310/+10 region for further analysis.

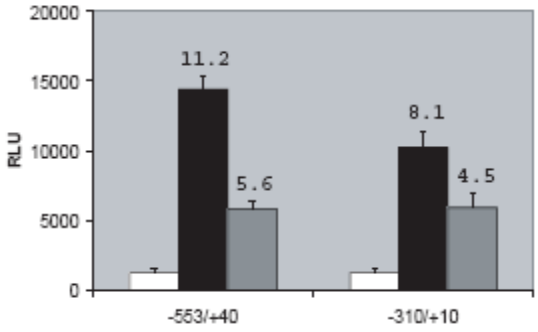

Figure 4-5. -310/+10 region retains most of the promoter activity.
-310/+10 region of mouse Sod2 promoter is highly induced by HIF-2α.
Numbers on top of each bar represents fold-induction compared to reporter alone activity.
Black bars: HIF-2α ,
Grey bars: FOXO3a-A3

Mutational analysis of transcription-factor binding sites in core core mSod2 promoter region

We started analysis of the -310/+10 region by mutating all three HREs (HRE3-5). Although, we did not observe any change in fold-activation of the

mutant promoter compared to wild-type, absolute activity of the mutant in the presence of HIF-2α was much lower (40%) than wild-type promoter (Figure 4-6). This result may indicate a role for those HREs (HRE 3-5) in the maintenance of basal expression levels of SOD2 gene. On the other hand, maintenance of inducibility by HIF-2α suggests that the mechanism of HIF-2α action is independent of its possible binding to the mutated HREs, although other factors that bind these mutated sites may increase the efficiency of HIF-2α action. The next question was whether HIF-2α interacts with other transcription factors / co-activators to mediate its effects on the mouse *Sod2* promoter. Therefore we identified and mutated possible transcription factor binding sites that seems to be conserved within -310/+10 region of the mouse SOD2 promoter (Figure 4-4).

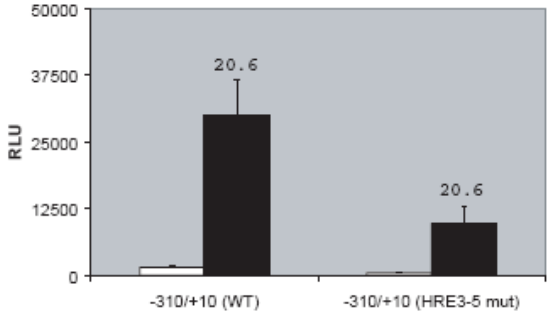

Figure 4-6. HRE3-5 mutant
Although mutation of HREs 3, 4, and 5 reduces promoter activity in the presence of HIF-2α, because the basal activity is also reduced, fold-elevation by HIF-2α remains same.
Numbers on top of each bar represents fold-induction compared to reporter alone activity.
Black bars: HIF-2α ,
Grey bars: FOXO3a-A3

Site-directed mutagenesis of single sites revealed that some of these sites (-80Sp1, -5ARE1) may be necessary for basal activity but they affect upregulation of the mouse Sod2 promoter by HIF-2α only minimally (Table 4-1).

Only -30Sp1 and -20AP4 mutation caused a substantial reduction (50%) in both absolute activity of the promoter in the presence of HIF-2α and fold-elevation over the empty vector.

Table 4-1. Absolute activities (RLU) of and fold-elevation of mutant Sod2 promoter constructs

Mutation	Abs. Activity (%)	Fold Elevation (%)
HRE 3-5	32	100
-85 AP2	64	75
-80 Sp1	39	81
-60 AP2	70	95
-45 HNF4	157	98
-30 Sp1	48	*51
-20 AP4	62	*68
-5 ARE1	67	105

Discussion

Both HIF-1α and HIF-2α bind to HREs (RCGTG) within 5' promoters or 3' enhancers of their target genes to upregulate their expression. Therefore, we cloned the genomic region 1.5 kb upstream to the transcriptional start site of the mouse *Sod2* gene and showed that this region can be induced by HIF-2α in HEK293 cells. Subsequently, we identified five consensus HRE sites upstream of the transcriptional start site and mutated those HREs (HRE 1-5). However, mutation of HREs 1-5 within the mouse *Sod2* promoter region caused only a partial reduction in both the absolute activity (RLU) and fold-elevation (compared to empty vector) of the mutant promoter activity by HIF-2α, compared to wild-type. Interestingly, mutation of only HRE 3-5 caused a dramatic decrease in absolute activity of the promoter, but it did not affect fold-elevation at all. Because

HRE1-5 and HRE3-5 were compared to different controls - -553/+40 and -310/+10, respectively-, we cannot say whether HREs 1-2 are more important for HIF-2α action or not.

Step-wise reduction of promoter mouse *Sod2* activity after 5' deletions and single-site mutations suggest that multiple sites play a role in the regulation of *Sod2* promoter by HIF-2α. It may be necessary to mutate multiple sites at once to observe a complete loss of HIF-2α effect on the *Sod2* promoter. The -30 Sp1 site seems to be the best candidate for a possible interaction site between Sp1 and HIF-2α. Interestingly, interaction between hypoxia/HIFs and Sp1/Sp3 have already been reported to be involved in transcriptional processes: a functional interaction between HIF-1α and Sp1/Sp3 on the retinoic acid receptor-related orphan receptor α4 (ROR α4) promoter is essential for hypoxic induction of the RORα4 gene (Miki, Ikuta et al. 2004). A similar interaction between HIF-2α and Sp1 may be responsible for the up-regulation of *Sod2* promoter in response to increased SO production. It is also possible that some other transcriptional co-activator, such as C/EBP, AP-1 or HNF-4, which are already known to interact with HIFs at various promoters (i.e. Lactate dehydrogenase A, VEGF and Epo) (Ebert and Wong 1995; Firth, Ebert et al. 1995; Galson, Tsuchiya et al. 1995; Damert, Ikeda et al. 1997), may mediate the effects of HIF-2α on *Sod2* promoter.

Further studies are required to better understand the mode of regulation of the mouse *Sod2* promoter by HIF-2α. Chromatin immunoprecipitation (ChIP) assays on the mouse *Sod2* promoter may prove to be useful to find out whether

endogenous HIF-2α interacts with Sp1 or other transcription factor/co-activators to activate the mouse *Sod2* promoter.

CHAPTER FIVE

MATERIALS AND METHODS

Mouse Studies:

All animal procedures were in accordance with guidelines established by the Institutional Animal Care and Use Committee (IACUC) of the University of Texas Southwestern Medical Center at Dallas. *Epas1*$^{-/-}$ mice were obtained from crosses of 129S6/SvEvTac and C57BL/6J strains heterozygous for the *Epas1* gene (Scortegagna, Ding et al. 2003). Mice housed in a standard 12 h light :12 h dark cycle were fed *ad libitum* with chow containing 4% fat (for mating pairs) or 11% fat (for pregnant females and newborn mice up to one month old).

MnTBAP Rescue Experiments

Rescue experiments were performed with intraperitoneal injections of 20−50 μg MnTBAP (Calbiochem) per 50 μl prepared in phosphate-buffered saline. Injections for newborns began on postnatal day 3 and continued once daily until postnatal day 24−28. Injections for pregnant females began seven days after mating and continued once daily through the day of delivery. Dosing for newborns and pregnant females was 10 μg per g body weight per day (Scortegagna, Ding et al. 2003).

Histological studies

For complete blood cell counts, blood samples were collected from ketamine-xylazine anesthetized mice by retro-orbital punctures or inferior vena cava cannulation just before euthanasia. Data represents information gathered from ten pairs of mice using automated cell counts done by an outside facility (LabCorp).

For β-galactosidase staining, wild-type or *Epas1*$^{-/-}$ mice were perfused with 4% paraformaldehyde in phosphate-buffered saline by cardiac perfusion techniques. Select organs were removed and postfixed for one additional hour before manipulations. Bone marrow left *in situ* was decalcified before Giemsa staining. Samples were embedded in paraffin for further sectioning when indicated.

Organs (heart, liver, skeletal muscle) were sectioned by vibratome before staining them with β-galactosidase, embedding and sectioning, and imaging (40 x fields). Hematoxylin and eosin staining was carried out on paraformaldehyde-fixed, paraffin-embedded samples (40x fields), oil red O staining on frozen sections (40x fields for initial histological studies; 20x fields for rescue experiments) and SDH or COX staining of skeletal muscle preparations on frozen soleus (SDH) or gastrocnemius (COX) samples (Seligman, Karnovsky et al. 1968; Dubowitz 1973). Samples were imaged under identical conditions. Post-hoc image adjustments were made, if needed, with identical modification of parameters for wild-type and *Epas1*$^{-/-}$ samples (Scortegagna, Ding et al. 2003).

These studies were performed in collaboration with John A. Shelton and James M. Richardson of the Department of Pathology, UTSWMC.

Ultrastructural studies

Select tissues were removed promptly from euthanized mice, minced and placed at room temperature in Fix Buffer (137 mM NaCl, 4 mM KCl, 2 mM $CaCl_2$, 100 mM MOPS, pH 7.4, 2.5 mM EM-grade glutaraldehyde) for 24 h with gentle rocking. Samples were washed sequentially with Fix Buffer and then with Rinse Buffer (137 mM NaCl, 4 mM KCl, 2 mM $CaCl_2$, 10 mM MOPS, pH7.4), equilibrated overnight in multiple washes with Rinse Buffer, postfixed (for 1 h in 1% OsO_4, 7% uranyl acetate) and dehydrated in graded ethanol before embedding in Spurr or Lowicryl resin. Specimens were sectioned at a thickness of 80 nm using a Reichert Ultracut S ultramicrotome, sections were placed on copper 200 mesh thin bar grids, stained with ethanolic uranyl acetate/Luft's lead citrate and examined with an electron microscope (JEOL 1200EX II Transmission Electron Microscope). Images were captured with a digital AMT CCD.

For mitochondrial morphometric determinations, liver, heart and soleus samples from three pairs of wild-type and *Epas1*$^{-/-}$ mice were examined by electron microscopy. Ultrathin sections (70−90 nm) were cut, transverse or slightly oblique to the fiber axis for skeletal muscle or heart, and stained with ethanolic uranyl acetate/Luft's lead citrate. Three randomly selected blocks for each tissue sample from each pair (for a total of nine blocks per tissue per genotype) were examined at a final magnification of 10,000x to determine

mitochondrial number and area. Area was determined using NIH Image and DrawPlus image analysis software. Mitochondrial area fraction was calculated as the total mitochondrial area in a designated cell, divided by the area of the cell, multiplied by 100% for a total of 50 cells from each tissue sample per genotype (Scortegagna, Ding et al. 2003). These studies were performed in collaboration with Frederick Thurmond of the Department of Internal Medicine, UTSWMC.

Superoxide anion studies

For qualitative assessment of superoxide anion levels, dihydroethidine staining was carried out on 6-μm-thick frozen liver sections obtained from freshly frozen samples. Frozen sections were incubated on glass slides for 30 min at 37 °C in dark with 2 μM dihydroethidine hydrochloride (Molecular Probes) in Krebs-HEPES solution. The sections were immediately photographed using a confocal microscope with CCD image-capture technology and the digital images were adjusted equivalently posthoc to distinguish areas of high signal intensity (which appear in yellow) from background intensity (labeled red).

For quantitative assessment of superoxide anion generation rates, mitochondrial extracts were prepared from *Epas1*$^{-/-}$ or wild-type mouse liver using mitochondria prepared by differential centrifugation. Liver samples were immediately removed from cervically dislocated mice, the blood was removed, liver was minced in ice-cold P buffer (250 mM sucrose, 10 mM Tris-HCl, pH 7.4, 1 mM EDTA) and then rinsed with P buffer until clear. Minced liver samples were homogenized in five volumes of P buffer, transferred to microfuge tubes, spun at

1,000 g for 5 min at 4 °C to pellet cell debris and nuclei and then the supernatant was transferred to new microfuge tubes. The resultant supernatant was spun at 10,000 g for 10 min at 4 °C to pellet the mitochondria, washed twice with ice-cold P buffer, wiped with Kimwipes between rinses to remove lipid residues. The supernatant was decanted and the mitochondrial pellets were flash-frozen in liquid nitrogen and stored at -80 °C.

To prepare SMP, frozen mitochondrial pellet were resuspended in 1 ml of 30 mM potassium phosphate buffer, pH 7.4, sonicated for four cycles on ice (30 s on/30 s off), spun at 5,000 g for 10 min at 4 °C to remove unbroken mitochondria and finally spun it at 100,000 g for 20 min at 4 °C to pellet the SMP. The SMP pellet was dissolved in 1 ml of 100 mM potassium phosphate buffer, pH 7.4, and homogenized again. The protein concentration of the homogenate was determined by the BCA assay (Pierce).

Superoxide generation rates were measured using ferricytochrome c reduction with acetylated cytochrome c as a substrate (Ku, Brunk et al. 1993). The use of acetylated cytochrome c increases specificity for the ferricytochrome c reduction assay by inhibiting reduction of cytochrome c by mitochondrial or microsomal reductases and its subsequent oxidation by mitochondrial oxidase (Ernster and Dallner 1995). The sample reaction (1 ml) contained 50−100 µg mitochondrial protein, 1 µM antimycin A, 12.5 µM rotenone and 10 µM acetylated cytochrome c. The reaction was started with addition of 7.5 mM potassium succinate and the absorbance at 550 nm was measured every minute for 15 min at 37 °C in a thermoregulated cuvette holder. Superoxide dismutase (200 units

ml^{-1}) was added to samples prepared in parallel to identify the SOD-sensitive rate of acetylated cytochrome c reduction and, hence, the portion attributable to superoxide-mediated reduction. The change in absorbance was normalized as a function of time (ΔA_{550} min^{-1}) to protein content (mg) and divided by the extinction coefficient for acetylated cytochrome c (27.7 μM^{-1} cm^{-1}) to determine the superoxide generation rate (μM min^{-1} mg^{-1}). The data presented depicts the means of duplicate experiments using four independent *Epas1*$^{-/-}$ and wild-type pairs in each experiment (Scortegagna, Ding et al. 2003).

Measurement of serum and urine metabolites, acyl-carnitine species

For serum analysis, we processed samples at the Dallas Children's Hospital Pathology Laboratory for routine electrolyte determinations. Urinary organic acids were identified and quantified as their trimethylsilyl derivatives by gas chromatography−mass spectrometry. Concentrations of urinary organic acids were measured and expressed as relative ratios (internal standard of 100 $\mu mol\ l^{-1}$ for each metabolite).

To characterize the acyl-carnitine profiles, 20 μl of serum was mixed with 300 μl of methanolic internal standards (final concentration of 1.3 μM acetyl carnitine, 0.53 μM palmitoyl carnitine and 0.27 μM all other internal standards), dried down under nitrogen at 40 °C, resuspended in 100 μl of 3 M HCl in n-butanol (Regis) and derivatized it at 65 °C for 15 min. After cooling, the tubes were dried under nitrogen and reconstituted them with 100 μl acetonitrile before

analyzing it by liquid chromatography/electrospray tandem mass spectrometry (LC/MS/MS) using a Perkin Elmer Sciex API 2000 setup (Applied Biosystems). Data are expressed as relative intensity (percentage) versus mass/charge ratio in atomic mass units. The following tri-deuterated analogs of native compounds (H.J. ten Brink, University Hospital, Amsterdam) were purchased and used as internal standards: [$^2H_3$]-carnitine, [$^2H_3$]-acetylcarnitine (C2), [$^2H_3$] propionylcarnitine (C3), [$^2H_3$]-butyrylcarnitine (C4), [$^2H_3$]-octanoylcarnitine (C8), [$^2H_3$]- dodecanoylcarnitine (C12) and [$^2H_3$]-hexadecanoylcarnitine (C16). Unlabeled acyl-carnitine standards were purchased from a commercial vendor (Sigma Chemical).

Procedures to Isolate Liver Mitochondria*:*

(a) *Oxygen Consumption Studies, Krebs Cycle Enzyme Acitivities, Mitochondrial NADH Oxidase Activity, Mitochondrial ATPase Activity and Mitochondrial GSH Measurements:* One month-old mice were used for isolation of liver mitochondria. Mice were cervically dislocated and a small piece of liver was immediately freeze-clamped for ATP, lactate, and pyruvate measurements. Liver mitochondria were isolated by differential centrifugation as described previously (Kokoszka, Coskun et al. 2001). Briefly, the remainder of the liver was weighed, minced in ice-cold PBS, and washed to remove blood. All steps were performed on ice or at 4 ˚C. The washed liver was placed in 15 vol:wt ice-cold Buffer H1 (225 mM mannitol, 75 mM sucrose, 10 mM MOPS, 1 mM EGTA and 0.5 % fatty-acid-free BSA, pH 7.2). The minced liver was homogenized gently with three

strokes in a Potter-Elvehjem homogenizer. The homogenate was centrifuged at 1,000 g for 7.5 min. The supernatant was carefully transferred to a new tube and centrifuged at 10,000 g for 10 min. The pellet was washed once with Buffer H2 (Buffer H1 without EGTA) and pelleted at 10,000 g for 7.5 min. The final pellet was resuspended in 200-300 µl of Buffer H2 with a rubber policeman and gently homogenized with a 1 ml Teflon-glass homogenizer (Wheaton Science Products, Millville, NJ). Protein concentration was determined using a BCA Assay Kit (Pierce, Rockford, IL). The suspension was used either immediately for polarographic oxygen consumption studies, for mitochondrial glutathione measurements, or was frozen at -80 ˚C for mitochondrial ATPase assays.

(b) *Liver OXPHOS Enzyme Activities:* Liver was washed in 0.15 M KCl, blotted, weighed and minced in 10 vol:weight Homogenization Buffer (120 mM KCl, 5 mM $MgCl_2$, 1mM EGTA, 20 mM HEPES, 0.5 % fatty-acid free BSA, and 50 units/ml heparin, pH 7.2). Minced liver was homogenized with Tenbrock homogenizer by hand. The homogenate was centrifuged at 1,000 g for 15 min at 4 ˚C. Aliquots of the homogenate was snap-frozen in liquid nitrogen, and stored at -80 ˚C for Complex I+III (NADH:ubiquinone reductase, NUR) or Complex III (ubiquinol:cytochrome c reductase, UCCR) activity assays. The remainder of the supernatant was freeze-thawed three times in liquid nitrogen and kept on ice during Complex II (succinate dehydrogenase, SDH), Complex IV (cytochrome c oxidase, COX) and Citrate Synthase (CS) assays.

(c) *mtPTP Opening Assay and Membrane Potential:* Liver was weighed, washed in ice-cold PBS, and homogenized in 5 vol:wt Isolation Buffer (0.18 M KCl, 10

mM EDTA, 10 mM HEPES pH 7.4, 0.5% fatty acid free BSA and one tablet/10 ml Roche Complete, Mini, EDTA-free protease inhibitor - Roche, Indiana, IN) with a Teflon-glass homogenizer. The homogenate was centrifuged at 600 g for 10 min and the supernatant again centrifuged at 600g for 10 min. To pellet the mitochondrial fraction, the supernatant was centrifuged at 8,500 g for 15 min. The pellet was washed twice with Washing Buffer (0.18 M KCl, 10 mM HEPES, pH 7.4) at 8,500 g for 10 min. The mitochondrial pellet was homogenized with a Teflon-glass homogenizer and protein concentration was determined by using a BCA assay kit (Pierce, Rockford, IL).

mtPTP Opening Assay:

Mitochondria (0.25 mg protein) was incubated with 1 ml Incubation Buffer (0.25 M sucrose, 10 mM Tris-10 mM MOPS, pH 7.4, 50 mM EGTA, 10 mM succinate, 1 mM potassium phosphate buffer, pH was adjusted to 7.4). MPTP opening was monitored at 540 nm immediately following the addition of 250 μM Ca^{2+} as described previously (Yan, Christians et al. 2002). Readings were obtained every one or two minutes and stopped at twenty minutes. These studies were performed in collaboration with Liang –Jun Yan of the Department of Pharmacology & Neuroscience, University of North Texas Health Science Center.

Determination of Liver Mitochondrial Membrane Potential:

Mitochondrial pellet was solubilized with a loose-fitting Teflon-glass homogenizer in Membrane Potential Buffer (0.2 M sucrose, 20 mM HEPES, 20 mM KCl, pH 7.2). Protein concentration was determined by Bradford Assay (Bio-Rad, Hercules, CA) and mitochondrial membrane potential was determined as described previously (Akerman and Wikstrom 1976). Briefly, mitochondrial suspension (0.5 mg protein) was adjusted to 6μM rotenone, 0.38 mM EDTA and 9.6 μM safranine. The adjusted mitochondrial suspension was incubated at RT for 2 min. A baseline was recorded from 350 nm to 650 nm. After addition of ATP to a final concentration of 1.5 mM, readings were recorded again and the difference between two readings was used to calculate the membrane potential. These studies were performed in collaboration with Liang –Jun Yan of the Department of Pharmacology & Neuroscience, University of North Texas Health Science Center.

Polarographic Measurement of Oxygen Consumption:

Oxygen consumption of isolated liver mitochondria was measured as described previously (Estabrook 1967; Kokoszka, Coskun et al. 2001) using a Clark-type oxygen electrode in a magnetically stirred 1.6 ml chamber at 30 ˚C. Mitochondrial suspension (one to two mg protein) was added to the oxygen electrode chamber containing Buffer W (225 mM mannitol, 75 mM sucrose, 5 mM KH_2PO_4, 10 mM KCl, 10 mM Tris-Cl, pH 7.2). After one min, either succinate (3.1 mM final concentration) in the presence of rotenone (5 μM final concentration) or glutamate plus malate (3.1 mM each) was added. Two to three

minutes later, State III respiration was initiated with the addition of ADP to a final concentration of 0.28 mM. State IV respiration rate was calculated as the oxygen consumption rate after all ADP was consumed. Two or three additions of ADP were performed until all oxygen was consumed. Respiratory Control Ratio (RCR) was calculated as the ratio of state III to state IV respiratory rates.

Assay of OXPHOS Enzymes:

(a) *NADH:ubiquinone reductase (NUR)* activity was measured as described by previously (Taylor and Turnbull 1997). Frozen 1000 g supernatant was thawed, diluted in 20 mM KH_2PO_4, pH 7.2, and mixed with 500 µl Assay Buffer (3mM KCN, 5mM $MgCl_2$, 75 µM coenzyme Q1, 0.13 mM NADH, 4 µg/ml antimycin, 35 mM potassium phosphate buffer, 2.5 mg/ml BSA, pH 7.2) in a cuvette at 30 ˚C. Oxidation of NADH was followed at 340 nm before and after addition of 4 µg/ml rotenone. Activity of NUR was calculated for a time period of no less than 0.7 min.

(b) *Succinate dehydrogenase (SDH)* activity was measured by the decrease in absorbance of dichlorophenolindophenol (DCPIP) at 600 nm, coupled to oxidation of succinate to fumarate by SDH, as described (Fischer, Ruitenbeek et al. 1985). Briefly, 1-2 µl of sample was incubated in a total volume of 50 µl of 50 mM potassium phosphate, pH 7.0 and 15 mM succinate, pH 7.5 at 30 ˚C for 20 min. Then, KCN, DCPIP and PES were added to final concentrations of 15 mM, 100 µM, 6 mM, respectively. Reduction of DCPIP to $DCPIPH_2$ was followed at

600 nm. Activity of SDH was calculated by using the extinction coefficient for DCPIP at 600 nm (19.1 mM^{-1} cm^{-1}).

(c) *Ubiquinol:cytochrome c reductase (UCCR)* activity was assayed as described previously (Taylor and Turnbull 1997). Reduction of cytochrome c (III) is coupled to oxidation of ubiquinol-2 and the increase in absorbance at 550 nm is followed. The reaction mix consisted of 3 mM KCN, 15 µM cytochrome c, 0.6 mM n-dodecyl-β-D-maltoside, 2 µg/ml rotenone, 60 µM ubiquinol-2 with and without sample, run in parallel. Activity of UCCR was calculated by using the extinction coefficient of reduced cytochrome c at 550 nm (20 mM^{-1} cm^{-1}).

(d) *Cytochrome c oxidase (COX)* activity was determined as described previously (Wharton and Tzagoloff 1967). In this assay, oxidation of reduced cytochrome c by COX was followed by a decrease in absorbance at 550 nm. Sample was diluted 1:10 vol:vol in 50 mM Potassium phosphate, 250 mM sucrose and 0.5 % taurodeoxycholic acid, pH 7.0. Reaction mix included 50 mM potassium phosphate, 10 µM reduced cytochrome c and sample. An extinction coefficient of 20 mM^{-1} cm^{-1} was used to calculate the rate of cytochrome c oxidation.

(e) *Citrate synthase (CS)* acitivity was assayed as described previously (Srere 1969). Release of CoASH was followed at 25 ˚C by increasing absorbance at 412 nm due to reaction of CoASH with 5,5'-dithiobis-2-nitro-benzoic acid (DTNB, Ellman's reagent) to yield yellow colored TNB (5-thio-2-nitro-benzoic acid). Reaction mix consisted of 0.1 mM DTNB, 0.3 mM acetyl-CoA, 0.5 mM oxaloacetate and mitochondria sample diluted 1:10 vol:vol in 50 mM potassium phosphate, 250 mM sucrose, 0.5% taurodeoxycholic acid, pH 7.0 in order to

break open the mitochondrial membranes and release citrate synthase. An extinction coefficient of 13.6 mM^{-1} cm^{-1} was used to calculate the rate of TNB formation and CS activity. Marguerite Gunder, Nadine Romain and Ron M. Haller of the Institute for Exercise and Environmental Science, Dallas, Texas provided expertise in these enzyme activity determinations.

Mitochondrial NADH Oxidase Assay

Mitochondrial suspension was thawed on ice and its concentration was adjusted to 0.5 mg/ml with 10 mM MOPS, pH 7.25. The suspension was sonicated as described for the previous two assays. The reaction mixture consisted of 10 mM MOPS (pH 7.25), 1 µM cytochrome c, 50 µM NADH and 50 µg SMP. NADH oxidase activity was calculated by using the extinction coefficient for NADH (6.22 M^{-1} cm^{-1}).

Mitochondrial Aconitase, Fumarase and α-KGDH Assays

Mitochondria was isolated as described in (a) and kept frozen at -80 ˚C. Aconitase and fumarase activities were measured spectrophotometrically, as described by (Racker 1950; Krebs and Holzach 1952; Melov, Coskun et al. 1999), except that reactions were run at 30 ˚C. Mitochondrial suspension was thawed on ice and its concentration adjusted to 0.05 mg/ml with 25 mM KH_2PO_4, and 0.5 mM EDTA, pH 7.25, containing 0.01 % Triton X-100. Diluted mitochondria were sonicated for 5 sec, cooled for 10 sec, repeated three times, at 30% output level (Fisher Scientific Sonic Dismembrator 550 Model, Pittsburgh,

PA). Formation of cis-aconitate was followed at 240 nm in 50 mM Tris-Cl (pH 7.4), 0.6 mM $MnCl_2$ and 20 mM isocitrate. An extinction coefficient for cis-aconitate of 3.6 mM^{-1} cm^{-1} was used to calculate the aconitase activity. Fumarase activity was measured in 30 mM potassium phosphate (pH 7.4), 0.1 mM EDTA and 5 mM malate. An extinction coefficient for fumarate of 2.4 mM^{-1} cm^{-1} was used to calculate the fumarase activity.

α-KGDH activity was measured as described (Nulton-Persson and Szweda 2001). The same SMP preparations was incubated with 5 mM $MgCl_2$, 20 μM rotenone, 2.5 mM α-ketoglutarate, 0.1 mM CoA, 0.2 mM thiamine pyrophosphate and 1 mM NAD^+, mM KH_2PO_4, and 0.5 mM EDTA, pH 7.25, and 0.01 % Triton X-100. Reduction of NAD^+ was followed at 340 nm and α-KGDH activity was calculated by using the extinction coefficient for NADH (6.22 M^{-1} cm^{-1}).

Preparation of Submitochondrial Particles (SMPs) for ATPase Sssay:

SMPs (EDTA-particles) were prepared as described (Lee and Ernster 1968) with modifications as indicated. All steps were performed on ice or at 4 ˚C. Frozen mitochondrial suspension was thawed on ice and its concentration adjusted to 20 mg/ml with 0.25 M sucrose. EDTA was added to a final concentration of 2 mM and the pH was increased to 8.0-8.5 with addition of 0.1 N NaOH. The mitochondrial suspension was sonicated for 10 sec, cooled for 30 sec and sonicated for 10 sec, at 30% output level (Fisher Scientific Sonic Dismembrator 550 Model, Pittsburgh, PA). One ml of ddH_20 was added and the

unbroken mitochondria were pelleted at 10,600 g for 10 min in a tabletop centrifuge. The supernatant was carefully transferred to a 5 ml ultracentrifuge tube and centrifuged at 105,000 g (48,000 rpm on a Beckman 70.1 Ti rotor) for 1 hour. The supernatant was discarded and the pellet washed with 500 µl of 0.25 M sucrose at 105,000 g for 40 min. The final pellet was resuspended in 50-125 µl of 0.25 M sucrose, frozen at -80 ˚C, and assayed within a week of preparation.

Mitochondrial ATPase Assay:

Mitochondrial ATPase activity was measured by modification of the method described previously (Fiske and Subbarow 1925). Thirty µg SMP or 1, 1.5, 2, 4, 6 mM KH_2PO_4 standards were incubated in Assay Buffer (50 mM KCl, 5 mM $MgCl_2$, 20 mM Tris-Cl, pH 7.4 and 1.25 µM rotenone) at 37 ˚C for 5 min. ATPase activity was stimulated by addition of Mg-ATP to a final concentration of 1 mM. Oligomycin (2 µM final) and ouabain (1 mM final) was used to determine non-mitochondrial ATPase activity (< 5 %). The reaction was stopped at t=2 min and t=4 min by addition of 1/5 vol of 30 % PCA and vortexing. After 5 min incubation on ice, suspensions were centrifuged at 10,000 g for 5 min and the supernatant used immediately. To measure phosphate, supernatant was incubated at RT in the presence of 3.3 mM sodium orthovanadate and 3.3 mM ammonium molybdate. Absorbance was measured at 400 nm after 5 min and ATPase activity was calculated as the difference in phosphate amounts between t = 2 min and t = 4 min time points, normalized to protein and time.

Measurement of Cellular and Mitochondrial GSH/GSSG:

(a) *Preparation of Mitochondrial Extracts:* Freshly isolated mitochondria were washed in Buffer W (225 mM mannitol, 75 mM sucrose, 5 mM KH_2PO_4, 10 mM KCl, 10 mM Tris-Cl, pH 7.2) at 10,000 g for 7.5 min. The mitochondrial pellet was resuspended in 50-125 µl of Buffer W. 5-10 µl of the suspension was incubated in 25 mM succinate at 37 ˚C for 5 min. Freshly prepared, ice-cold 10% sulfosalisylic acid (SSA) + 0.5 mM EDTA (1:1 vol:vol) was added and vortexed. After incubation on ice for 5 min, 2 volumes of ddH_2O were added and the extract centrifuged at 10,600 g in a tabletop centrifuge. The supernatant was carefully transferred to a new tube and kept at -20 ˚C for less than one week before assaying.

(b) *Preparation of Liver Extracts:* Snap frozen liver was thawed and rinsed in ice-cold PBS. Ice-cold 10% SSA +0.5 mM EDTA (3:1 vol:weight) was added and the liver was homogenized, kept on ice for 5 min and centrifuged at 10,600 g in a tabletop centrifuge. The supernatant was carefully transferred to a new tube and kept at -20 ˚C for less than one week prior to assaying.

(c) *Assay of GSH/GSSG:* Total and oxidized glutathione was determined according to (Tietze 1969) modified for a 96-well plate assay. In this method, 100 µl mitochondrial or whole liver extract was derivatized for 1 hour with 2 µl 97 % 2-vinylpyridine and 4-5 µl 50% triethanolamine, at a final pH 6-7. Derivatized, non-derivatized extracts and the respective standards were added to the GSH Assay Buffer (0.143 mM sodium phosphate buffer, 6.3 mM EDTA, 300 µM NADPH, pH 7.5) in duplicates on a 96-well plate. DTNB was added as quickly as possible

(6mM for GSH, 12 mM for GSSG, final concentration) and readings at 412 nm were taken for 5 min. After addition of GSH-reductase (from Baker's yeast; 1.5 u/ml for GSH, 3 u/ml for GSSG) readings at 412 nm were taken every 3-4 min for 20-30 min. GSH and GSSG concentrations were calculated according to standard curves.

Perchloric Acid Extraction:

Freeze-clamped samples were kept at -80 ˚C until perchloric acid (PCA) extraction as (Passonneau and Lowry 1993). Liver sample was taken out of -80 ˚C and placed in a mortar filled with liquid nitrogen to prevent thawing. Frozen sample was finely pulverized in mortar and transferred to ice-cold, preweighed 30 % PCA (3:1 vol:wt) and the total weight recorded. After incubation at 4 ˚C for 10 min, ice-cold ddH_2O (2.5 vol:vol) was added and the sample was centrifuged at 5,000 g for 10 min at 4 ˚C. Supernatant was carefully transferred to a new tube and the pH was adjusted to 6-7 with dropwise addition of freshly prepared 2 M $KHCO_3$. The supernatant was frozen overnight and the pH was readjusted the day following extraction. Extract was centrifuged at 5,000 g for 10 min at 4 ˚C and the final supernatant was stored at -80 ˚C.

Measurement of Lactate and Pyruvate:

The day following PCA extraction, pyruvate was measured spectrophotometrically by the method of (Czok and Lamprecht 1974). Briefly, extract was incubated in a reaction mix consisting of 3 mM EDTA, 0.1 mM NADH

and 300 mM triethanolamine-HCl buffer, pH 7.6. The reaction was started with addition of LDH (5 µg/ml final concentration; from rabbit muscle). Oxidation of NADH was followed by decrease in absorbance at 340 nm. Pyruvate amount was calculated using the extinction coefficient for NADH (6.22 M^{-1} cm^{-1}). The same extracts were used for determination of lactate (Gutmann and Wahlefeld 1974). The reaction mixture consisted of PCA extract, 0.43 M glycine, 0.34 M hydrazine, and 2.75 mM NAD^+. The reaction was started with the addition of LDH (10 µg/ml final concentration) and the increase in absorbance due to reduction of NAD^+ to NADH was followed at 340 nm. Lactate amount was calculated using the extinction coefficient for NADH (6.22 M^{-1} cm^{-1}).

Transfection studies

Cat, Gpx1, Sod1 or Sod2 promoters were identified by homology analysis using human or rat promoter regions as a probe for the mouse genomic DNA database (National Center for Biotechnology Information or Celera mouse genomic database) and mouse RefSeq data (National Center for Biotechnology Information) to determine the start of transcription. The promoters were amplified while introducing a BglII or BamHI restriction site into the 5' untranslated region and a NheI restriction site in the 5' end of the promoter fragment. The AOE promoters (-746 to +76 for Cat, -1,402 to +31 for Gpx1, -1,616 to +128 for Sod1 and -1,452 to +40 for Sod2) were cloned into the luciferase reporter plasmid pGL3-basic (Promega) for subsequent use in transfection studies. Where

needed, gaps in the available mouse genomic database sequence were filled by sequencing of the subcloned promoter regions (Sod1).

The expression plasmid pIRES-hrGFP (Stratagene) was used as the expression plasmid vector backbone for the HIF-2α expression constructs. The HIF-2α expression construct contained a full-length human EPAS1 (wild-type) cDNA with a single hemagglutinin tag in-frame at the C terminus. Human embryonic kidney 293 cells (HEK293) passaged in 48-well plates were cot-ransfected with DNA-liposome complexes formed with 15 ng of either pGL3-basic reporter alone (luc) or the indicated mouse AOE promoter in the pGL3-basic background, 200 or 400 ng of either pIRES-hrGFP or the wild-type HIF-2α expression plasmid and 1 μl Lipofectamine 2000 (Invitrogen Life Technologies). After 30 min, the DNA-liposome complexes were added to HEK293 cells (90% or 30% confluent, 48-well plates) and cells were incubated overnight. Luciferase activity was determined from cellular extracts using a Berthold Sirius luminometer.

Activation of AOE promoter constructs were compared to activation of the positive control plasmid HRE-tk-luc (hypoxia responsive element triplet concatamer fused upstream of a minimal thymidine kinase promoter) or to the negative control plasmid Hsp90-luc (heat shock protein 90 promoter). Each transfection was carried out in quadruplicate for the indicated sample. Data are presented as activation relative to promoter construct alone. The data shown represents the mean of five independent sets of transfections.

Molecular studies

Tissue samples were obtained from freshly euthanized mice to generate total RNA and prepare first-strand cDNA. Quantitative real-time RT-PCR technique was used to identify changes in gene expression of candidate genes with SYBR-green using an ABI Prism 7700 sequence detection system instrument and software (Applied Biosystems). The genes examined included the four primary AOE genes (Cat, Gpx1, Sod1 and Sod2) and a housekeeping gene for the internal standard (Actb). Primers designed to span introns were used and validated before use by analysis of template titration and dissociation curves. Expression of select genes in samples from Epas1$^{-/-}$ versus wild-type mice were compared using the threshold cycle method normalized to Actb (User Bulletin Number 2, Perkin-Elmer Life Sciences). The data are the overall mean of 3−5 set means, each generated from triplicate real-time RT-PCR data points. Each independent set consists of two different RNA pools with each pool generated from the tissues of three one-month-old mice matched for genotype, gender, age and litter. The primers sequences are available on request, for a list of primers used, see Table 5-1.

Table 5-1. Primer list for real-time RT-PCR

gene name	Description	primers	product length	Accession #	Exon
Cat/Cas1	Catalase	CCGAGTCTCTCCATCAGGTTT	69bp	L25069	Exon5
		TCATGTGCCGGTGACCAT			Exon6
Gpx1	Glutathione peroxidase 1	CGGTTTCCCGTGCAATC	68bp	NM_008160	Exon1
		GAGGGAATTCAGAATCTCTTCAT			Exon2
SOD1	superoxide dismutase 1	TTTTAATCCTCACTCTAAGAAACATGGT	70bp	XM_128337	Exon3
		ACATTGCCCAGGTCTCCAA			Exon4
SOD2	superoxide dismutase 2	CTCTGGCCAAGGGAGATGTT	70bp	NM_013671	Exon2
		GTCCCCCACCATTGAACTTC			Exon3
CHOP10	Ddit3	CACCACACCTGAAAGCAGAAC	65bp	NM_007837	exon4
		GGTGAAAGGCAGGGACTCA			Exon4/5
MT-II	Metallothionein 2	AAATGTACTTCCTGCAAGAAAAGCT	71bp	AK002567	exon2/3
		CAGCCCTGGGAGCACTTC			Exon3

To determine MnSOD levels, 25 μg of protein from Epas1$^{-/-}$ and wild-type liver mitochondrial preparations was subjected to SDS-PAGE. Western-blot analysis of mitochondrial protein extracts was carried out using a commercially available rabbit polyclonal antibody to MnSOD (Stressgen), a peroxidase-conjugated goat antibody to rabbit IgG (Pierce) and a chemiluminescent developer (Pierce). For porin analyses, a mouse monoclonal antibody to human porin (anti-porin 31HL, Calbiochem) was used at a dilution of 1:1,000 for the primary antibody and a peroxidase-conjugated goat antibody to mouse IgG as the secondary antibody. Western-blot images were acquired by film and the images were stored digitally for later analysis (Scortegagna, Ding et al. 2003).

BIBLIOGRAPHY

Agani, F. H., P. Pichiule, et al. (2000). "The role of mitochondria in the regulation of hypoxia-inducible factor 1 expression during hypoxia." J Biol Chem **275**(46): 35863-7.

Akerman, K. E. and M. K. Wikstrom (1976). "Safranine as a probe of the mitochondrial membrane potential." FEBS Lett **68**(2): 191-7.

Bardos, J. I. and M. Ashcroft (2005). "Negative and positive regulation of HIF-1: a complex network." Biochim Biophys Acta **1755**(2): 107-20.

Bruick, R. K. and S. L. McKnight (2001). "A conserved family of prolyl-4-hydroxylases that modify HIF." Science **294**(5545): 1337-40.

Carmeliet, P., V. Ferreira, et al. (1996). "Abnormal blood vessel development and lethality in embryos lacking a single VEGF allele." Nature **380**(6573): 435-9.

Chandel, N. S., E. Maltepe, et al. (1998). "Mitochondrial reactive oxygen species trigger hypoxia-induced transcription." Proc Natl Acad Sci U S A **95**(20): 11715-20.

Chandel, N. S., D. S. McClintock, et al. (2000). "Reactive oxygen species generated at mitochondrial complex III stabilize hypoxia-inducible factor-1alpha during hypoxia: a mechanism of O2 sensing." J Biol Chem **275**(33): 25130-8.

Compernolle, V., K. Brusselmans, et al. (2002). "Loss of HIF-2alpha and inhibition of VEGF impair fetal lung maturation, whereas treatment with VEGF prevents fatal respiratory distress in premature mice." Nat Med **8**(7): 702-10.

Cramer, T., Y. Yamanishi, et al. (2003). "HIF-1alpha is essential for myeloid cell-mediated inflammation." Cell **112**(5): 645-57.

Czok, R. and W. Lamprecht (1974). "Pyruvate, Phosphoenolpyruvate and D-glycerate-2-phosphate." In: Methods of Enzymatic Analysis, 2nd ed. (Bergmeyer HU Ed) Verlag Chemie, Weinheim: 1446-1451.

Damert, A., E. Ikeda, et al. (1997). "Activator-protein-1 binding potentiates the hypoxia-inducible factor-1-mediated hypoxia-induced transcriptional activation of vascular-endothelial growth factor expression in C6 glioma cells." Biochem J **327 (Pt 2)**: 419-23.

Dhar, S. K., B. C. Lynn, et al. (2004). "Identification of nucleophosmin as an NF-kappaB co-activator for the induction of the human SOD2 gene." J Biol Chem **279**(27): 28209-19.

Drapier, J. C. and J. B. Hibbs, Jr. (1986). "Murine cytotoxic activated macrophages inhibit aconitase in tumor cells. Inhibition involves the iron-sulfur prosthetic group and is reversible." J Clin Invest **78**(3): 790-7.

Dubowitz, V. (1973). "Morphological studies on transplanted muscle between normal and dystrophic animals." J Physiol **231**(2): 59P.

Ebert, S. N. and D. L. Wong (1995). "Differential activation of the rat phenylethanolamine N-methyltransferase gene by Sp1 and Egr-1." J Biol Chem **270**(29): 17299-305.

Elson, D. A., G. Thurston, et al. (2001). "Induction of hypervascularity without leakage or inflammation in transgenic mice overexpressing hypoxia-inducible factor-1alpha." Genes Dev **15**(19): 2520-32.

Ema, M., K. Hirota, et al. (1999). "Molecular mechanisms of transcription activation by HLF and HIF1alpha in response to hypoxia: their stabilization and redox signal-induced interaction with CBP/p300." Embo J **18**(7): 1905-14.

Epstein, A. C., J. M. Gleadle, et al. (2001). "C. elegans EGL-9 and mammalian homologs define a family of dioxygenases that regulate HIF by prolyl hydroxylation." Cell **107**(1): 43-54.

Ernster, L. and G. Dallner (1995). "Biochemical, physiological and medical aspects of ubiquinone function." Biochim Biophys Acta **1271**(1): 195-204.

Estabrook, R. W. (1967). "Mitochondrial respiratory control and the polarographic measurement of ADP : O ratios." Methods in Enzymology (Estabrook RW and Pullman ME, Eds.) **10**: 41-47.

Fernandez-Checa, J. C., N. Kaplowitz, et al. (1997). "GSH transport in mitochondria: defense against TNF-induced oxidative stress and alcohol-induced defect." Am J Physiol **273**(1 Pt 1): G7-17.

Firth, J. D., B. L. Ebert, et al. (1995). "Hypoxic regulation of lactate dehydrogenase A. Interaction between hypoxia-inducible factor 1 and cAMP response elements." J Biol Chem **270**(36): 21021-7.

Fischer, J. C., W. Ruitenbeek, et al. (1985). "Differential investigation of the capacity of succinate oxidation in human skeletal muscle." Clin Chim Acta **153**(1): 23-36.

Fiske, C. and Y. Subbarow (1925). "The colorimetric determination of phosphorous." J Biol Chem **66**: 375-400.

Fridovich, I. (1999). "Fundamental aspects of reactive oxygen species, or what's the matter with oxygen?" Ann N Y Acad Sci **893**: 13-8.

Friedman, J. S., V. I. Rebel, et al. (2001). "Absence of mitochondrial superoxide dismutase results in a murine hemolytic anemia responsive to therapy with a catalytic antioxidant." J Exp Med **193**(8): 925-34.

Galson, D. L., T. Tsuchiya, et al. (1995). "The orphan receptor hepatic nuclear factor 4 functions as a transcriptional activator for tissue-specific and hypoxia-specific erythropoietin gene expression and is antagonized by EAR3/COUP-TF1." Mol Cell Biol **15**(4): 2135-44.

Gong, Y. and F. H. Agani (2005). "Oligomycin inhibits HIF-1alpha expression in hypoxic tumor cells." Am J Physiol Cell Physiol **288**(5): C1023-9.

Graham, B. H., K. G. Waymire, et al. (1997). "A mouse model for mitochondrial myopathy and cardiomyopathy resulting from a deficiency in the

heart/muscle isoform of the adenine nucleotide translocator." Nat Genet **16**(3): 226-34.

Griffith, O. W. and A. Meister (1985). "Origin and turnover of mitochondrial glutathione." Proc Natl Acad Sci U S A **82**(14): 4668-72.

Gutmann, I. and A. W. Wahlefeld (1974). "L-(+)-Lactate, Determination with lactate dehydrogenase and NAD." In: Methods of Enzymatic Analysis, 2nd ed. (Bergmeyer HU, Ed), Verlag Chemie, Weinheim: 1464-1468.

Hu, C. J., L. Y. Wang, et al. (2003). "Differential roles of hypoxia-inducible factor 1alpha (HIF-1alpha) and HIF-2alpha in hypoxic gene regulation." Mol Cell Biol **23**(24): 9361-74.

Huang, J., Q. Zhao, et al. (2002). "Sequence determinants in hypoxia-inducible factor-1alpha for hydroxylation by the prolyl hydroxylases PHD1, PHD2, and PHD3." J Biol Chem **277**(42): 39792-800.

Huang, T. T., E. J. Carlson, et al. (2001). "Genetic modification of prenatal lethality and dilated cardiomyopathy in Mn superoxide dismutase mutant mice." Free Radic Biol Med **31**(9): 1101-10.

Iyer, N. V., L. E. Kotch, et al. (1998). "Cellular and developmental control of O2 homeostasis by hypoxia-inducible factor 1 alpha." Genes Dev **12**(2): 149-62.

Jaakkola, P., D. R. Mole, et al. (2001). "Targeting of HIF-alpha to the von Hippel-Lindau ubiquitylation complex by O2-regulated prolyl hydroxylation." Science **292**(5516): 468-72.

Kietzmann, T. and A. Gorlach (2005). "Reactive oxygen species in the control of hypoxia-inducible factor-mediated gene expression." Semin Cell Dev Biol.

Kokoszka, J. E., P. Coskun, et al. (2001). "Increased mitochondrial oxidative stress in the Sod2 (+/-) mouse results in the age-related decline of mitochondrial function culminating in increased apoptosis." Proc Natl Acad Sci U S A **98**(5): 2278-83.

Kops, G. J., T. B. Dansen, et al. (2002). "Forkhead transcription factor FOXO3a protects quiescent cells from oxidative stress." Nature **419**(6904): 316-21.

Krebs, H. A. and O. Holzach (1952). "The conversion of citrate into cis-aconitate and isocitrate in the presence of aconitase." Biochem J **52**(3): 527-8.

Ku, H. H., U. T. Brunk, et al. (1993). "Relationship between mitochondrial superoxide and hydrogen peroxide production and longevity of mammalian species." Free Radic Biol Med **15**(6): 621-7.

Lando, D., I. Pongratz, et al. (2000). "A redox mechanism controls differential DNA binding activities of hypoxia-inducible factor (HIF) 1alpha and the HIF-like factor." J Biol Chem **275**(7): 4618-27.

Lebovitz, R. M., H. Zhang, et al. (1996). "Neurodegeneration, myocardial injury, and perinatal death in mitochondrial superoxide dismutase-deficient mice." Proc Natl Acad Sci U S A **93**(18): 9782-7.

Lee, C. and L. Ernster (1968). "Studies of the energy-transfer system of submitochondrial particles. I. Competition between oxidative phosphorylation and the energy-linked nicotinamide-adenine dinucleotide transhydrogenase reaction." Eur J Biochem **3**(4): 385-90.

Lee, C. P. (1995). "Biochemical studies of isolated mitochondria from normal and diseased tissues." Biochim Biophys Acta **1271**(1): 21-8.

Li, Y., T. T. Huang, et al. (1995). "Dilated cardiomyopathy and neonatal lethality in mutant mice lacking manganese superoxide dismutase." Nat Genet **11**(4): 376-81.

Lu, H., R. A. Forbes, et al. (2002). "Hypoxia-inducible factor 1 activation by aerobic glycolysis implicates the Warburg effect in carcinogenesis." J Biol Chem **277**(26): 23111-5.

Mastrangelo, I. A., A. J. Courey, et al. (1991). "DNA looping and Sp1 multimer links: a mechanism for transcriptional synergism and enhancement." Proc Natl Acad Sci U S A **88**(13): 5670-4.

Matecki, S., G. Py, et al. (2002). "Effect of prolonged undernutrition on rat diaphragm mitochondrial respiration." Am J Respir Cell Mol Biol **26**(2): 239-45.

Maxwell, P. H. (2005). "Hypoxia-inducible factor as a physiological regulator." Exp Physiol **90**(6): 791-7.

Maxwell, P. H., M. S. Wiesener, et al. (1999). "The tumour suppressor protein VHL targets hypoxia-inducible factors for oxygen-dependent proteolysis." Nature **399**(6733): 271-5.

Melov, S., P. Coskun, et al. (1999). "Mitochondrial disease in superoxide dismutase 2 mutant mice." Proc Natl Acad Sci U S A **96**(3): 846-51.

Melov, S., J. A. Schneider, et al. (1998). "A novel neurological phenotype in mice lacking mitochondrial manganese superoxide dismutase." Nat Genet **18**(2): 159-63.

Metzen, E., U. Berchner-Pfannschmidt, et al. (2003). "Intracellular localisation of human HIF-1 alpha hydroxylases: implications for oxygen sensing." J Cell Sci **116**(Pt 7): 1319-26.

Meyrick, B. and M. A. Magnuson (1994). "Identification and functional characterization of the bovine manganous superoxide dismutase promoter." Am J Respir Cell Mol Biol **10**(1): 113-21.

Miki, N., M. Ikuta, et al. (2004). "Hypoxia-induced activation of the retinoic acid receptor-related orphan receptor alpha4 gene by an interaction between hypoxia-inducible factor-1 and Sp1." J Biol Chem **279**(15): 15025-31.

Munnich, A., A. Rotig, et al. (1996). "Clinical presentations and laboratory investigations in respiratory chain deficiency." Eur J Pediatr **155**(4): 262-74.

Nemoto, S. and T. Finkel (2002). "Redox regulation of forkhead proteins through a p66shc-dependent signaling pathway." Science **295**(5564): 2450-2.

Nulton-Persson, A. C., D. W. Starke, et al. (2003). "Reversible inactivation of alpha-ketoglutarate dehydrogenase in response to alterations in the mitochondrial glutathione status." Biochemistry **42**(14): 4235-42.

Nulton-Persson, A. C. and L. I. Szweda (2001). "Modulation of mitochondrial function by hydrogen peroxide." J Biol Chem **276**(26): 23357-61.

O'Rourke, J. F., Y. M. Tian, et al. (1999). "Oxygen-regulated and transactivating domains in endothelial PAS protein 1: comparison with hypoxia-inducible factor-1alpha." J Biol Chem **274**(4): 2060-71.

Park, S. K., A. M. Dadak, et al. (2003). "Hypoxia-induced gene expression occurs solely through the action of hypoxia-inducible factor 1alpha (HIF-1alpha): role of cytoplasmic trapping of HIF-2alpha." Mol Cell Biol **23**(14): 4959-71.

Passonneau, J. V. and O. H. Lowry (1993). In: Enzymatic Analysis: A Practical Guide. Humana Press, Totowa, NJ.

Peng, J., L. Zhang, et al. (2000). "The transcription factor EPAS-1/hypoxia-inducible factor 2alpha plays an important role in vascular remodeling." Proc Natl Acad Sci U S A **97**(15): 8386-91.

Pollard, P. J., J. J. Briere, et al. (2005). "Accumulation of Krebs cycle intermediates and over-expression of HIF1{alpha} in tumours which result from germline FH and SDH mutations." Hum Mol Genet **14**(15): 2231-9.

Porntadavity, S., Y. Xu, et al. (2001). "TPA-activated transcription of the human MnSOD gene: role of transcription factors Sp-1 and Egr-1." DNA Cell Biol **20**(8): 473-81.

Pugh, C. W., J. F. O'Rourke, et al. (1997). "Activation of hypoxia-inducible factor-1; definition of regulatory domains within the alpha subunit." J Biol Chem **272**(17): 11205-14.

Racker, E. (1950). "Spectrophotometric measurements of the enzymatic formation of fumaric and cis-aconitic acids." Biochim Biophys Acta **4**(1-3): 211-4.

Richard, D. E., E. Berra, et al. (2000). "Nonhypoxic pathway mediates the induction of hypoxia-inducible factor 1alpha in vascular smooth muscle cells." J Biol Chem **275**(35): 26765-71.

Rifai, Z., S. Welle, et al. (1995). "Ragged red fibers in normal aging and inflammatory myopathy." Ann Neurol **37**(1): 24-9.

Ryan, H. E., J. Lo, et al. (1998). "HIF-1 alpha is required for solid tumor formation and embryonic vascularization." Embo J **17**(11): 3005-15.

Salceda, S. and J. Caro (1997). "Hypoxia-inducible factor 1alpha (HIF-1alpha) protein is rapidly degraded by the ubiquitin-proteasome system under normoxic conditions. Its stabilization by hypoxia depends on redox-induced changes." J Biol Chem **272**(36): 22642-7.

Schafer, F. Q. and G. R. Buettner (2001). "Redox environment of the cell as viewed through the redox state of the glutathione disulfide/glutathione couple." Free Radic Biol Med **30**(11): 1191-212.

Schroedl, C., D. S. McClintock, et al. (2002). "Hypoxic but not anoxic stabilization of HIF-1alpha requires mitochondrial reactive oxygen species." Am J Physiol Lung Cell Mol Physiol **283**(5): L922-31.

Scortegagna, M., K. Ding, et al. (2003). "Multiple organ pathology, metabolic abnormalities and impaired homeostasis of reactive oxygen species in Epas1-/- mice." Nat Genet **35**(4): 331-40.

Seagroves, T. N., H. E. Ryan, et al. (2001). "Transcription factor HIF-1 is a necessary mediator of the pasteur effect in mammalian cells." Molecular & Cellular Biology **21**(10): 3436-44.

Selak, M. A., S. M. Armour, et al. (2005). "Succinate links TCA cycle dysfunction to oncogenesis by inhibiting HIF-alpha prolyl hydroxylase." Cancer Cell **7**(1): 77-85.

Seligman, A. M., M. J. Karnovsky, et al. (1968). "Nondroplet ultrastructural demonstration of cytochrome oxidase activity with a polymerizing osmiophilic reagent, diaminobenzidine (DAB)." J Cell Biol **38**(1): 1-14.

Semenza, G. L. (2004). "Hydroxylation of HIF-1: oxygen sensing at the molecular level." Physiology (Bethesda) **19**: 176-82.

Semenza, G. L. and G. L. Wang (1992). "A nuclear factor induced by hypoxia via de novo protein synthesis binds to the human erythropoietin gene enhancer at a site required for transcriptional activation." Mol Cell Biol **12**(12): 5447-54.

Sies, H. and T. P. Akerboom (1984). "Glutathione disulfide (GSSG) efflux from cells and tissues." Methods Enzymol **105**: 445-51.

Srere, P. A. (1969). "Citrate synthase : [EC 4.1.3.7. Citrate oxaloacetate-lyase (CoA-acetylating)]." In: Methods in Enzymology (Lowenstein JM, Ed.), Academic Press, New York City **13**: 3-11.

St Clair, D. (2004). "Manganese superoxide dismutase: genetic variation and regulation." J Nutr **134**(11): 3190S-3191S.

Storz, P., H. Doppler, et al. (2005). "Protein kinase D mediates mitochondrion-to-nucleus signaling and detoxification from mitochondrial reactive oxygen species." Mol Cell Biol **25**(19): 8520-30.

Taylor, B. L. and I. B. Zhulin (1999). "PAS domains: internal sensors of oxygen, redox potential, and light." Microbiol Mol Biol Rev **63**(2): 479-506.

Taylor, R. W. and D. M. Turnbull (1997). In: Organelle Diseases-Clinical Features, Diagnosis, Pathogenesis and Management (Applegarth DA, Dimmick JE and Hall JG, Eds.) Chapman and Hall, London: 341-350.

Tian, H., R. E. Hammer, et al. (1998). "The hypoxia-responsive transcription factor EPAS1 is essential for catecholamine homeostasis and protection against heart failure during embryonic development." Genes Dev **12**(21): 3320-4.

Tian, H., S. L. McKnight, et al. (1997). "Endothelial PAS domain protein 1 (EPAS1), a transcription factor selectively expressed in endothelial cells." Genes Dev **11**(1): 72-82.

Tietze, F. (1969). "Enzymic method for quantitative determination of nanogram amounts of total and oxidized glutathione: applications to mammalian blood and other tissues." Anal Biochem **27**(3): 502-22.

Tretter, L. and V. Adam-Vizi (2000). "Inhibition of Krebs cycle enzymes by hydrogen peroxide: A key role of [alpha]-ketoglutarate dehydrogenase in limiting NADH production under oxidative stress." J Neurosci **20**(24): 8972-9.

Van Remmen, H., C. Salvador, et al. (1999). "Characterization of the antioxidant status of the heterozygous manganese superoxide dismutase knockout mouse." Arch Biochem Biophys **363**(1): 91-7.

Veech, R. L., L. V. Eggleston, et al. (1969). "The redox state of free nicotinamide-adenine dinucleotide phosphate in the cytoplasm of rat liver." Biochem J **115**(4): 609-19.

Wallace, D. C. (2001). "Mouse models for mitochondrial disease." Am J Med Genet **106**(1): 71-93.

Wang, G. L., B. H. Jiang, et al. (1995). "Hypoxia-inducible factor 1 is a basic-helix-loop-helix-PAS heterodimer regulated by cellular O2 tension." Proc Natl Acad Sci U S A **92**(12): 5510-4.

Wang, G. L., B. H. Jiang, et al. (1995). "Effect of altered redox states on expression and DNA-binding activity of hypoxia-inducible factor 1." Biochem Biophys Res Commun **212**(2): 550-6.

Wang, V., D. A. Davis, et al. (2005). "Differential gene up-regulation by hypoxia-inducible factor-1alpha and hypoxia-inducible factor-2alpha in HEK293T cells." Cancer Res **65**(8): 3299-306.

Wenger, R. H., D. P. Stiehl, et al. (2005). "Integration of oxygen signaling at the consensus HRE." Sci STKE **2005**(306): re12.

Wharton, D. C. and A. Tzagoloff (1967). In: Methods in Enzymology. (Estabrook RW and Pullman ME, Eds.), Academic Press, New York City **10**: 245-50.

Wiesener, M. S., J. S. Jurgensen, et al. (2003). "Widespread hypoxia-inducible expression of HIF-2alpha in distinct cell populations of different organs." Faseb J **17**(2): 271-3.

Wiesener, M. S., H. Turley, et al. (1998). "Induction of endothelial PAS domain protein-1 by hypoxia: characterization and comparison with hypoxia-inducible factor-1alpha." Blood **92**(7): 2260-8.

Williams, M. D., H. Van Remmen, et al. (1998). "Increased oxidative damage is correlated to altered mitochondrial function in heterozygous manganese superoxide dismutase knockout mice." J Biol Chem **273**(43): 28510-5.

Xu, Y., S. Porntadavity, et al. (2002). "Transcriptional regulation of the human manganese superoxide dismutase gene: the role of specificity protein 1 (Sp1) and activating protein-2 (AP-2)." Biochem J **362**(Pt 2): 401-12.

Yan, L. J., E. S. Christians, et al. (2002). "Mouse heat shock transcription factor 1 deficiency alters cardiac redox homeostasis and increases mitochondrial oxidative damage." Embo J **21**(19): 5164-72.

Yu, A. Y., L. A. Shimoda, et al. (1999). "Impaired physiological responses to chronic hypoxia in mice partially deficient for hypoxia-inducible factor 1alpha." J Clin Invest **103**(5): 691-6.

Zhu, C. H., Y. Huang, et al. (2001). "A family of AP-2 proteins down-regulate manganese superoxide dismutase expression." J Biol Chem **276**(17): 14407-13.

Zoratti, M. and I. Szabo (1995). "The mitochondrial permeability transition." Biochim Biophys Acta **1241**(2): 139-76.

VITAE

Yavuz Oktay was born in Izmir, TURKEY, on June 2, 1979, the son of Cevdet and Gulsum Oktay. He attended Esrefpasa Primary School and Fevzi Cakmak Secondary School in Izmir. After completing Izmir Ataturk Lisesi with high-honors in 1997, he entered the Molecular Biology and Genetics Department at Bilkent University, Ankara, TURKEY. He graduated from Bilkent University with a B.Sc. degree with honors in June 2001. He entered the Graduate School of Biomedical Sciences, Division of Basic Science, at the University of Texas Southwestern Medical Center at Dallas, in August 2001. He pursued a doctorate degree in the laboratory of Dr. Joseph A. Garcia. In December 2005, he obtained his doctorate degree from the Integrative Biology Graduate Program in the Graduate School of Biomedical Sciences at the University of Texas Southwestern Medical Center at Dallas.

Permanent Adress:

520/2 Sokak No.30 D.3, Yilmaz Apt.

Ucyol, Konak-Izmir 35270

TURKEY